Genetic Modulation of Lifespan: Dynamic Effects, Sex Differences, and Body Weight Trade-offs

Danny Arends[1], David G. Ashbrook[2], Suheeta Roy[2], Lu Lu[2], Zachary Sloan[2], Arthur G. Centeno[2], Kurt H. Lamour[3], João Pedro de Magalhães[4], Pjotr Prins[2], Karl W. Broman[5], Saunak Sen[6], Sarah J. Mitchell[7], Michael R. MacArthur[8], Özlem Altintas Akin[9], Johan Auwerx[10], Amandeep Bajwa[2,11], Vivian Diaz[13], David E. Harrison[12], Randy Strong[13], James F. Nelson[13], Khyobeni Mozhui[2,6], Evan G. Williams[14], Richard A. Miller[15], Robert W. Williams[2]

[1] Department of Applied Sciences, Northumbria University, Newcastle upon Tyne, UK
[2] Department of Genetics, Genomics and Informatics, University of Tennessee Health Science Center; Memphis, TN, USA
[3] Department of Entomology and Plant Pathology, The University of Tennessee, Knoxville, Knoxville, TN, USA
[4] Department of Inflammation and Ageing, University of Birmingham, Birmingham, UK
[5] Department of Biostatistics and Medical Informatics, University of Wisconsin-Madison; Madison, WI, USA
[6] Department of Preventive Medicine, University of Tennessee Health Science Center; Memphis, TN, USA
[7] Ludwig Princeton Branch, Princeton University; Princeton, NJ, USA
[8] Lewis-Sigler Institute for Integrative Genomics, Princeton University; Princeton, NJ, USA
[9] Department of Health Sciences and Technology, ETH Zurich, Zurich, Switzerland.
[10] Laboratory of Integrative Systems Physiology, Institute of Bioengineering, École Polytechnique Fédérale de Lausanne; Lausanne, Switzerland
[11] Department of Surgery, University of Tennessee Health Science Center; Memphis, TN, USA
[12] The Jackson Laboratory; Bar Harbor, ME, USA
[13] Barshop Institute for Longevity and Aging Studies, University of Texas Health San Antonio; San Antonio USA
[14] Luxembourg Centre for Systems Biomedicine, University of Luxembourg, Esch-sur-Alzette, Luxembourg
[15] Department of Pathology and Geriatrics Center, University of Michigan, Ann Arbor, MI 48109, USA

Email to R.W. Williams (labwilliams@gmail.com) and D. Arends (danny.arends@gmail.com)

The dynamics of lifespan are shaped by DNA variants that exert effects at different ages. We have mapped genetic loci that modulate age-specific mortality using a new actuarial method. We started with 6,438 pubescent mice and ended with a survivorship of 559 mice that lived to at least 1100 days of age. Twenty-nine *Vita* loci dynamically modulate lifespan and have strong age-delimited effects after correction for multiple tests. Fourteen loci have relatively steady but genotype-dependent effects on mortality from pubescence to old age and are candidate aging rate modulators. Other loci act most forcefully over shorter periods of life, and the polarities of their genetic effects often invert with age and differ by sex. We detect 41 epistatic interactions among these *Vita* loci, all exclusive to males or females, and with strong signatures of sexual reciprocity. A distinct set of 19 *Soma* loci shape the *negative* correlation between larger body size in young adults with their subsequent life expectancies. These loci are direct evidence that antagonistic pleiotropy modulates mortality early in life. Another set of 11 *Soma* loci shape the *positive* correlation between heavier body weight at older ages and longer life expectancies. We provide exemplars of how to move from maps to mechanisms for two tractable loci. Our findings provide a solid empirical bridge between evolutionary theories on aging and their molecular causes. The 59 loci are keys to understand the impact of interventions on healthy lifespan in mice and humans.

We do not yet understand genetic, molecular, cellular, and organismal processes that shape intrinsic variability in rates of aging, lifespan, and all-cause mortality in humans, mice, or other model organisms such as *Drosophila*[1–16]. While thousands of variants modulate risks of age-related diseases[17,18], the great majority influence proximate causes of death but not the core mechanisms that influence aging rates *per se*[19–23]. To disentangle causes from consequences and to define variants that modulate mortality across entire lifespans, we developed an actuarial approach that maps life expectancies of progressively older survivorships; from those that include all mice from pubescence upward, to cohorts made up only of those that lived to at least 1100 days; equivalent to a range from 12 to 94 years in humans[24,25]. This approach has been tested previously in *Drosophila*[26–29], but has not been applied systematically in any organism. The closest human parallels are biometric studies of age-dependent changes in heritability of lifespan in Scandinavian twin cohorts born between 1870 and 1910[30,31]. Our study is a complementary genetic dissection but at the level of discrete genetic effects—59 well-defined loci that dynamically influence mortality and lifespan. We address four sets of questions in geroscience:

1. When and how do genetic variants influence mortality rates? Which have effects consistent with modulating aging rates, which have transient effects consistent with specific diseases, which have effects only late in life?
2. Do loci conform to predictions of evolutionary theories of aging—the *disposable soma*, *mutation accumulation*, and *antagonistic pleiotropy* theories that posit early acting beneficial effects that improve fitness but that have neutral or deleterious effects on mortality late in life?
3. How do genetic variants influence sex differences on mortality during and after reproduction? Is there evidence of genotype-by-sex (GxS) and genotype-by-genotypes (GxG) interactions and antagonism? Are effects age-dependent?
4. What accounts for the negative association between body size early in life and lifespan? What specific loci operate, and at what ages does weight predict life expectancy?

To dissect the genetic contributions to lifespan we relied on the largest study of mouse aging—the National Institute on Aging's *Interventions Testing Program* (ITP)[32]. For over two decades, teams at three sites have used a highly diverse population of full genetic sibs called the *University of Michigan Heterogenous Cohort 3* (UM-HET3) to study the effects of drug interventions on longevity[32–34]. UM-HET3 mice are created by crossing first-generation hybrids of four fully inbred progenitors—BALB/cByJ (cBy or *C*), C57BL/6J (B6 or *B*), C3H/HeJ (C3 or *H*), and DBA/2J (D2 or *D*)—that have life expectancies from 600 days in D2 to 900 days in B6[35,36]. The UM-HET3 segregate for ~10 million DNA variants, a level of diversity matchings that of

humanity[37]. Between 2004 and 2013, the ITP took tissues from 13,200 pubescent mice at 42-days-of-age. We used 6,438 of these animals for genetics—excluding from the current study mice treated with dietary supplements such as rapamycin that extend lifespan. The sibship was aged to natural death in pathogen-free vivaria at the Jackson Laboratory, the University of Michigan, and the University of Texas Health San Antonio. Our findings are robust with respect to a decade-long experiment and environmental differences among sites.

In earlier work we mapped lifespan using 3,055 control mice and detected seven lifespan loci[38]. Here we have doubled sample size by adding 3,383 mice given supplements that did *not* affect lifespan. We quadrupled numbers of genetic markers and introduced a new actuarial method. As a result, we have increased numbers of lifespan loci *(Vita* type) four-fold. In addition, we mapped 30 loci of a new type that specifically influence the correlations between body weight and life expectancies in males and females (*Soma* type loci).

The dynamics of *Vita* and *Soma* loci are highly complex. Some act in early or late survivorships. A subset modulate expectancies uniformly and include DNA variants that act as pacemakers of aging[39]. Many loci have striking and even counterbalanced sex differences, as do their epistatic interactions. Some have effects predicted by the theory of antagonistic pleiotropy[40–42], while others have effects long after the reproductive phase and are more consistent with *mutation accumulation* and *disposable soma* theories[2,43,44].

Results

We analyzed life expectancies of 6,438 mice across 72 survivorships, each of which was generated by truncating upward in 15-day steps. The full survivorship includes all pubescent mice that entered the study between 2004 and 2013. The last survivorship includes only the subset of 559 of these mice that lived to between 1100 and 1456 days of age (Fig. 1a,b). We refer to survivorships by their truncation age (T-age). At the base truncation of T_{42} the sex difference in lifespans of UM-HET3 mice is 81 days (Fig. 1b). The mean lifespan for males is 806 ± 210 SD days, that for females is 887 ± 175 SD days. This difference is stable from T_{42} to T_{215} because so few mice die in the first 215 days of life—20 males and 13 females. In contrast, between 215 and 410 days many more males die than females—204 males and 18 females. This striking sex difference in early deaths produces the symmetric inflections in the actuarial effect size plot in Fig 1b. They are symmetric because they are normalized to the mean of both sexes combined at every T-age. By the T_{740} survivorship lifespans of males and females have converged precisely—946±2.7 and 946±2.4 SE days (Fig. 1b). The terminal survivorship of 277 males and 282 females have lifespans of 1166±3.2 and 1159±3.3 SE days. The T-age of a survivorship refers to an entire age *range*.

Actuarial truncation in a forward direction means that the oldest-old mice are embedded in every survivorship. Reverse truncation flips polarity by truncating from oldest to youngest and defines exitships. The $_{1099}T$ exitship consists of mice that died before 1100 days and complements the T_{1100} survivorship. The combination of forward, reverse, and two-sided truncations is useful to dissect causes of mortality in age-restricted

subpopulations. In this paper we focus only on forward truncation. The analysis of epistatic interactions is challenged by modest sample sizes in each of the 4x4 genotype classes. We therefore decided to limit our analysis to T_{42}, T_{365}, T_{740}, and T_{905}.

29 *Vita* loci defined by actuarial dissection of 72 survivorships

We resolved loci modulating mean lifespans of survivorships at a genome-wide false discovery rate <0.05 after applying a stringent Bonferroni correction and a Cauchy correction for actuarial time-series analysis (Table 1, Fig. 1, Methods). *Vita* loci have effects of 36 ± 12 days (d) on life expectancies that depend on sex and T-age (Table 1, Fig. 1c-f, Extended Data Figs. 1–2). Peak effects average 2.5 ± 0.9% of variance for females; 3.2 ± 0.5% for males. Linkage ranges from a low of about 4.1 LOD (*Vita5a*) to a high of 9.0 in males (*Vita4a*), and from a low of 4.1 (*Vita11b*) to a high of 8.1 in females (*Vita2c*). Confidence intervals of loci average 35 ± 19 Mb SD[45] with the smallest under 10 Mb (Table 1, Fig. 1d-f). *Vita* loci have age-delimited actuarial effects—not mechanistic effects—that average 349 ± 229 days SD (Table 1, average of *Duration* column) and range between 45 and 900 days.

Table 1. *Vita* loci modulate the dynamics of lifespan as a function of sex and survivorship

				Vita Positions (Mb, GRCm38) ¥					Survivorship T-Ages Δ						Effect Sizes			Sex Effects*			Epistatic Effects by Sex			Survivorship Summary	
	Locus	Peak LOD @	Cauchy –logP ^	Chr	Prox	Peak	Distal	Size (Mb)	From	Peak T-Age	To	Dura-tion	Max *N at Peak* §	Mean Life § (d)	Peak Var Male %	Peak Var Fem %	Max Peak Diff (d)	Sex Effects*	GxS at Peak LOD †	Max GxS at any T-age $	*Locus*	Interactions in Male ◊	Interactions in Female ◊	Type and Age of Main Effects **	See Extd Figs 1–2
1	***Vita1a***	**6.84**	3.64	**1**	0.0	**3.0**	8.0	8.0	42	**860**	935	893	3377	1002	5.7	3.4	30	C, F, M	0.78	1.40	***Vita1a***	11c	**6b**, **9a**, **11a**	Durable, Late Reversal (M F)	**a**
2	***Vita1b***	**7.91**	3.83	**1**	16.0	**24.0**	31.1	15.1	42	**695**	845	803	5056	930	4.4	2.2	37	C, F	0.78	0.78	***Vita1b***		6b, **9a**, **9b**	Durable, Late Reversal (M F)	**b**
3	***Vita1c***	**5.51**	3.14	**1**	101.4	**121.5**	148.6	47.2	42	**230**	335	308	3255	810	3.0	0.0	52	M	2.41	2.62	***Vita1c***	***3a***, 11c	2b	Early (M)	**c**
4	***Vita1d***	**5.47**	3.05	**1**	151.7	**167.1**	176.3	24.6	42	**230**	335	293	3379	810	0.9	0.0	54	M	2.28	2.28	***Vita1d***	**2c**, **9b**, **9c**	2b, 15b, **18a**	Early (M)	**d**
5	***Vita2a***	**5.54**	3.14	**2**	71.8	**89.2**	110.9	39.0	42	**140**	275	233	1548	807	2.9	5.6	70	M, F, X	**9.78**	9.78	***Vita2a***	13a, 14a		Early, Reversal (M), RAM (F)	**e**
6	***Vita2b***	**6.84**	3.51	**2**	110.9	**112.7**	130.9	20.0	575	**800**	890	315	4079	970	0.5	1.1	20	F, C,X, M	0.35	8.62	***Vita2b***	3a, **14b**	1c, 1d, 6a	Reversal (M), RAM (F)	**f**
7	***Vita2c***	**8.13**	4.61	**2**	132.8	**148.4**	158.4	25.6	42	**545**	665	623	2930	906	0.0	1.2	30	F, C, X	2.65	7.31	***Vita2c***	**1d**		Reversal (M), RAM (F)	**g**
8	***Vita3a°***	**4.26**	1.92	**3**	42.2	**83.8**	121.5	79.2	1055	**1070**	1100	45	368	1146	7.5	0.0	35	M, X	**3.07**	3.07	***Vita3a°***	**1c**, 2b	**5a**	Early, RAM, Rev (M), Durable (F)	**h**
9	***Vita4a***	**9.00**	4.84	**4**	38.9	**52.5**	63.3	24.3	42	**650**	710	668	2588	908	8.2	1.6	53	M, C, X	**2.98**	3.58	***Vita4a***			Mid, Reversal (M), Durable (F)	**i**
10	***Vita4b***	**4.43**	2.38	**4**	132.4	**154.3**	156.0	23.6	500	**635**	680	180	2652	900	2.5	0.0	33	M, X	**3.30**	3.64	***Vita4b***	**14b**	**12a**	Mid (M)	**j**
11	***Vita5a***	**4.05**	2.10	**5**	36.6	**67.6**	90.2	53.6	965	**1085**	1100	135	350	1149	8.0	0.0	36	M, X	**2.85**	2.91	***Vita5a***		**3a**, 17	Late (M)	**k**
12	***Vita6a***	**4.14**	2.93	**6**	97.3	**107.4**	122.3	25.0	42	**140**	560	518	3396	807	2.2	0.0	38	M, C	1.74	1.74	***Vita6a***	14a	2b, 11b	Early, Mid (M)	**l**
13	***Vita6b***	**5.27**	3.05	**6**	108.1	**132.8**	149.7	41.7	42	**320**	515	473	3296	823	2.6	0.0	47	M, X	**2.79**	2.79	***Vita6b***	**13a**, 15a	**1a**, 1b, 14a, 14b	Early, Mid, RAM (M)	**m**
14	***Vita9a***	**5.68**	3.75	**9**	13.4	**29.9**	44.7	31.2	42	**95**	725	683	2754	910	0.9	5.0	35	F, C, M, X	**5.80**	5.80	***Vita9a***		**1a**, **1b**	Early (M), Early, Mid, RAM, Rev (F)	**n**
15	***Vita9b***	**6.66**	3.28	**9**	95.3	**104.1**	116.5	21.2	935	**1025**	1055	120	1847	1112	6.5	9.0	24	C, F, M	1.21	2.11	***Vita9b***	**1d**, **17a**	**1b**	Early, Reversal, Late (M), Late (F)	**o**
16	***Vita9c***	**5.79**	3.20	**9**	108.1	**124.1**	124.4	16.3	920	**980**	1070	150	1990	965	1.1	1.4	20	C, M, X	2.73	2.73	***Vita9c***	**1d**, **17a**		Early, Reversal, Late (M), Late (F)	**p**
17	***Vita10a***	**4.48**	2.48	**10**	56.7	**72.8**	100.5	43.7	965	**980**	1010	45	1812	1078	5.8	0.2	23	C, M	0.86	1.33	***Vita10a***	14a		Late (M)	**q**
18	***Vita11a***	**4.21**	2.20	**11**	0.0	**5.6**	30.1	30.1	560	**635**	695	135	2652	901	3.4	0.0	35	M	1.86	1.86	***Vita11a***			Mid Reversal (M)	**r**
19	***Vita11b***	**4.07**	1.96	**11**	59.0	**82.2**	109.4	50.4	995	**1040**	1055	60	586	1114	0.0	9.1	29	F, X	1.86	3.45	***Vita11b***		**1a**, 14a	Durable, Late Reversal (F)	**s**
20	***Vita11c***	**4.91**	2.91	**11**	97.9	**113.7**	119.3	21.3	42	**42**	290	248	3332	806	1.7	0.2	44	M, X	**4.41**	4.71	***Vita11c***	1a, 1c, 13a		RAM (M)	**t**
21	***Vita12a***	**5.22**	3.01	**12**	99.6	**112.9**	120.1	20.6	530	**635**	695	165	5475	910	1.5	2.5	27	C	0.03	0.94	***Vita12a***		**4b**	Durable (M,) Durable (F)	**u**
22	***Vita13a***	**5.62**	3.36	**13**	47.9	**86.8**	114.9	67.0	42	**230**	410	368	6203	863	1.4	1.7	33	C, M	0.29	1.68	***Vita13a***	2a, 6b, 11c		RAM (M), Mid (F)	**v**
23	***Vita14a***	**6.08**	3.61	**14**	62.6	**70.8**	101.4	38.8	42	**42**	290	248	6438	844	2.8	1.2	48	C, M	1.62	1.69	***Vita14a***	2a, 6a,10a,17a	6b, 11a, **11b**	Early (M), RAM (F)	**w**
24	***Vita14b°***	**4.86**	2.87	**14**	78.4	**101.4**	120.3	41.9	42	**80**	290	248	3377	1006	2.1	0.4	18	C, M	0.22	1.80	***Vita14b***	**2b**, **4b**	6b	RAM (M), RAM (F)	**x**
25	***Vita15a***	**5.08**	2.89	**15**	55.5	**74.2**	88.4	32.9	785	**905**	950	165	3549	1023	5.7	1.9	21	C, M, X	1.36	3.25	***Vita15a***			Early, Mid, RAM (M), Durable (F,C)	**y**
26	***Vita15b***	**5.73**	3.14	**15**	99.3	**102.2**	104.0	4.7	42	**95**	275	233	3398	813	1.3	0.0	40	M, X	**4.11**	4.11	***Vita15b***	6b	1d	Early, Mid, Late (M)	**z**
27	***Vita17a***	**4.97**	3.07	**17**	0.0	**32.9**	73.7	73.7	440	**665**	740	300	5286	925	3.8	1.3	23	C, M	0.77	2.24	***Vita17a***	**9b**, **9c**,11b, 14a	5a	RAM (M)	**aa**
28	***Vita18a***	**4.56**	2.73	**18**	33.2	**52.5**	81.0	47.8	42	**140**	455	413	6431	858	1.5	1.6	28	C	1.49	1.63	***Vita18a***		**1d**	Early (M), RAM (F)	**ab**
29	***VitaXa***	**5.64**	3.28	**X**	0.0	**36.0**	69.8	69.8	42	**260**	485	443	3332	806	6.6	0.0	35	M	NA	NA	***VitaXa***			RAM (M)	**ac**

@ **Peak LOD** values are significant at *P* of .01, .05, and .10 with LODs of 4.65, 3.95, and 3.65, respectively.
^ **Cauchy –logP** values are significant at ≥ 1.5.
¥ ***Vita*** chromosomes (**Chr**) and **Positions** in megabases using GRCm38/mm11 assembly. **Peak** is the marker position with the highest LOD at **Peak T-age. Prox** and **Distal** are proximal and distal marker positions. **Size** of locus in **Mb** (megabases).
Δ **Survivorship T-Age**s in 15-day truncation steps over which *Vita* loci are regarded as having an impact on lifespan centered around the **Peak T-Age** that gave the **Peak LOD** for the first-listed **Sex Effects** entry.
§ **Max *N* at Peak** is the survivorship sample size at the ***Vita* Peak LOD** at the **Peak T-Age.** For example, for Vita1a this number is 3377 mice at T860 which had a **Mean Survival** of 1002 days.
% **Peak Var Fem** and **Peak Var Male** are percentages of variance the locus can account for in the survivorship with the **Peak LOD.** See Extended Data Fig. 3 for variances explained at all T-ages in both sexes.
* **Sex Effects** associated with high linkages: male (**M**), female (**F**), combined (**C**), and GxS effect (**X**). The order is given by LOD score from high to low. **Peak LOD** only applies to the first **Sex Effects** entry.
† **GxS LOD. Bold** values are significant with Bonferroni corrections at ≤.05 with LOD of ≥2.75 when tested at the **Peak LOD** marker and **Peak T-Age**.
$ **Max GxS LOD** in any T-age survivorship
◊ **Epistatic Effects by Sex : *Vita* loci** are isted with sufixes at LOD ≥3.8. **Bold font** for LOD ≥4.5.
** **Type and Age of Main Effect**s depend on sex as noted. See **Results** for explanations of *categories* and caveats. **Durable**: Effects to ≥T770; **RAM**: Gradual effect reduction to ≥T800; **Rev**: Effect reversals; **Early**: ≤T500, **Mid**: T500 to T845, **Late**: ≥T860.
° ***Vita3a*** and ***Vita14b*** are ARM loci with two T-ages with high LOD scoes. ***Vita3a*** has an early effect but LODs are significant only late males. The highest LOD for ***Vita14b*** is at T860 in combined data, but see Fig 2b for early peak LOD in males.

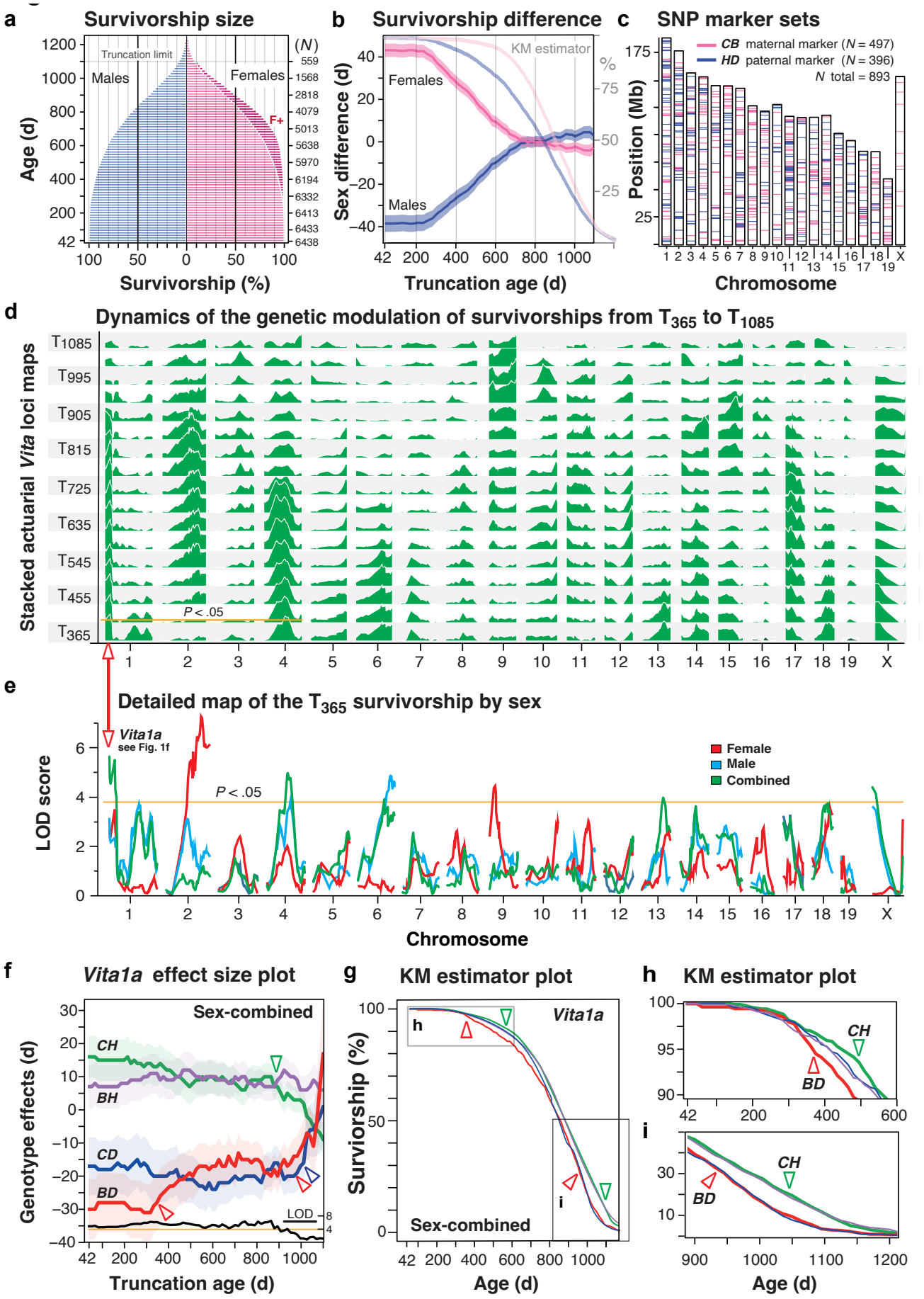
a
Survivorship size
Truncation limit
Males
Females
F+
(N)
Age (d)
Survivorship (%)
b
Survivorship difference
KM estimator
Females
Males
Sex difference (d)
Truncation age (d)
c
SNP marker sets
CB maternal marker (N = 497)
HD paternal marker (N = 396)
N total = 893
Position (Mb)
Chromosome
d
Dynamics of the genetic modulation of survivorships from T365 to T1085
Stacked actuarial Vita loci maps
T1085
T995
T905
T815
T725
T635
T545
T455
T365
P < .05
e
Detailed map of the T365 survivorship by sex
Vita1a
see Fig. 1f
Female
Male
Combined
LOD score
Chromosome
f
Vita1a effect size plot
Sex-combined
CH
BH
CD
BD
LOD
Genotype effects (d)
Truncation age (d)
g
KM estimator plot
Vita1a
Sex-combined
Surviorship (%)
Age (d)
h
KM estimator plot
CH
BD
i
Age (d)

Fig. 1 | Mortality, sex differences, and the *Vita* survivorship loci. a, Survivorships of mice stratified by the minimum inclusion age starting at a population of 6,438 at our base truncation age (T-age) of T_{42} and extending to a high of T_{1100}, This final survivorship has 559 mice. The first death was at 46 days, the last death at 1456 days. 364 more males (*blue bars*) were entered into the study, but by T_{530} n/sex was matched. *F+* denotes the proportional survival advantage of females (darker red bars, 4% at T_{365}). Truncation ages (left *y-axis*) and numbers of survivors on the right *y*-axis. **b,** Sex differences in mean lifespans of the T_{42} to T_{1100} survivorships. The 81-day difference at T_{42} is neutralized by T_{725}. Kaplan-Meier (KM) estimators for both sexes are superimposed. **c,** Ideogram of chromosomes and approximate megabase (Mb, GRCm38/mm10) of SNPs used to define maternal (*C* vs *B*) and paternal haplotypes (*H* vs *D*). **d,** Stacked survivorship maps for sex-combined data from T_{365} to T_{1085}. **e,** The map of T_{365} corresponds to the lowest tier of panel **d** but now with resolution of female (*red*), male (*blue*), and combined (*green*) plots. The *red triangle* marks the *Vita1a* locus. **f**, Actuarial genetic effect size plots from T_{42} to T_{1100}. The *y*-axis defines the mean lifespan differences of survivorships for the four genotypes as a function of truncation age (*x*-axis) relative to the average of all four genotypes. LOD scores are plotted above the *x* axis with an orange line at $P < .05$. The four **colored triangles** mark mortality inflection points in these plots associated with changes. **g,** KM estimator of survival stratified by genotypes of the same locus and genotypes with the four arrowheads positioned as in **f.** **h,i** are detailed views of the KM plot that resolve effects of genotypes and mortality rate changes at inflection points. More mice with *BD* genotypes die between 300 to 600 days, and again after 900 days. Inflections correspond to subtle differences in slopes of KM plots, although the change is clear in panel **h** for the *BD* genotype.

Dynamics of *Vita* loci

Effects of *Vita* loci on lifespan are highly age-dependent (Fig. 1a-f; Table 1, right-most column; Extended Data Figs 1–2). *Vita1a* and *Vita1b* have actuarial effects across almost all T-ages (Figs 1f, 2a). *Vita14b* has a smooth reduction in actuarial effects—a relative constant and converging slopes of the *BD* and *CH* genotype classes from T_{230} to T_{1100}. Others have transient effects. *Vita1c* acts only in survivorships that include adults younger than 500 days (Fig. 2c) whereas *Vita9b* and *Vita9c* act in the oldest decile (Fig. 2f). *Vita4a* has effects on survivorships that reverse between T_{410} and T_{800} days (Fig. 2e). The triangles in Fig. 1f-1 highlight points at which a disproportionate number of *BD* carriers die between 305 and 500 days in a first wave, and from 950 days onward in a second wave (Extended Data Figs 1a, 2a). Inflections in plots correspond to points on Kaplan-Meier curves at which genotype classes diverge or converge. A wave of higher of lower mortality in one genotype changes its subsequent difference in mean life expectancy compared to other classes (Fig. 1f-I, Fig. 2b). For this reason, the durability of the actuarial effects of *Vita1a* from T_{42} and T_{905} is paradoxically caused by genotype class differences in mortality of the oldest mice—higher mortality of the *CD* and *BD* classes starting at the inflection point in Fig. 1f marked by red and blue triangles near T_{950}. An important conclusion: the biological and mechanistic impact of *Vita* variants are generally greatest at inflections in actuarial plots (Fig. 2a-f, Extended Data Figs 1, 2). These are T-ages at which the third derivative has a high absolute value, with swings in life expectancy of entire survivorships that are as large as 5–15 days over just 45 days (Fig. 2e). In contrast, those *Vita* loci that have a comparatively constant slope from T_{42} to beyond T_{905} behave as expected of rate of aging modulators[10,39].

We have categorized the dynamics of *Vita* loci into four groups (Table 1, far right side):

1. **Loci with durable effects.** Five loci, such as *Vita1* (Fig. 1f) have uniform actuarial effects that are detected even in the T42 base population and out to at least T_{750} in one or both sexes (Table 1). Their uniformity of actuarial effects means they are powerful predictors of lifespan even in adolescence, but their mechanistic impact on aging and disease risk will not be detectible until late in life when they finally act.

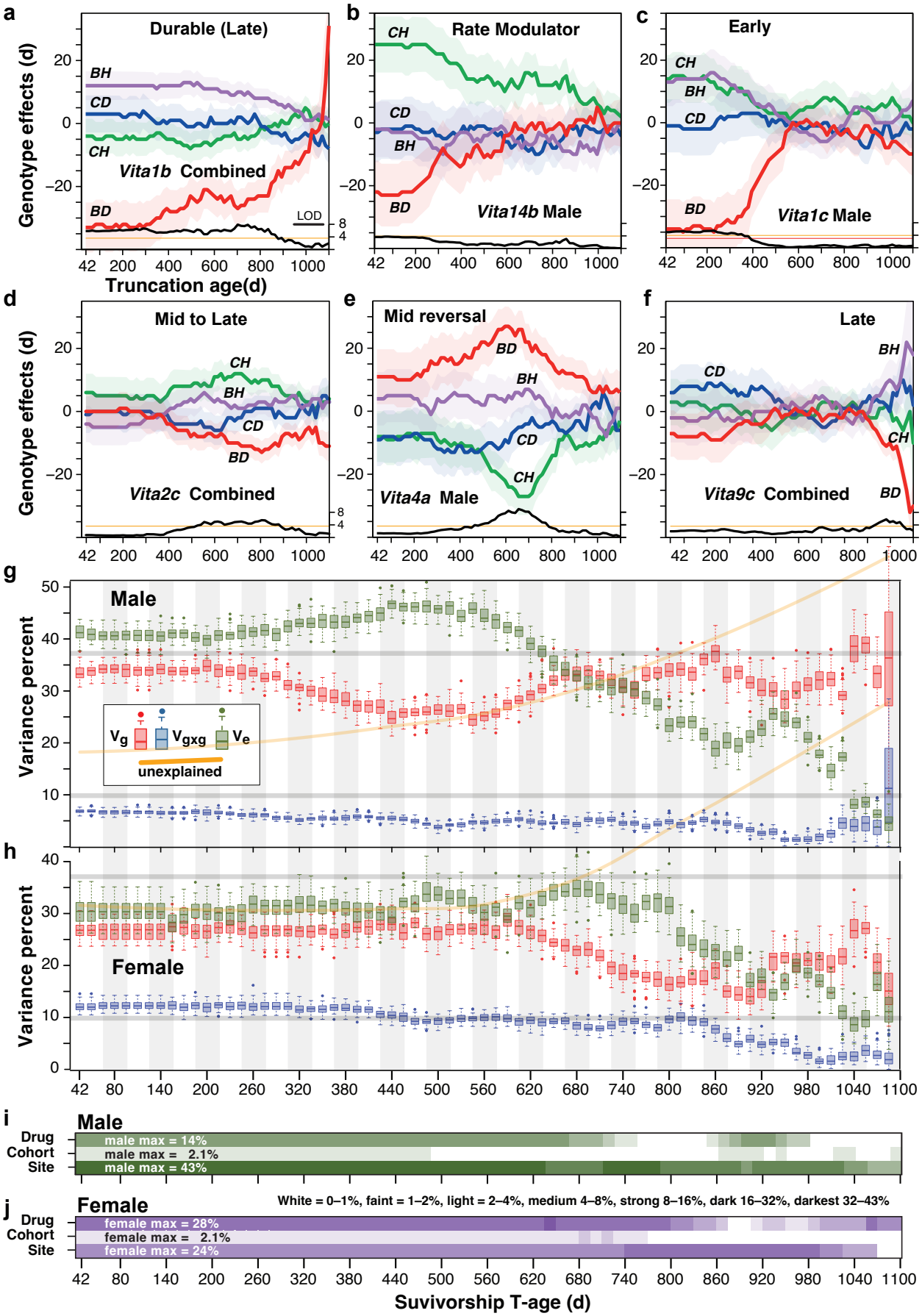
a
Durable (Late)
Genotype effects (d)
BH
CD
CH
BD
Vita1b Combined
LOD
b
Rate Modulator
CH
CD
BH
BD
Vita14b Male
c
Early
CH
BH
CD
BD
Vita1c Male
Truncation age(d)
d
Mid to Late
CH
BH
CD
BD
Vita2c Combined
e
Mid reversal
BD
BH
CD
CH
Vita4a Male
f
Late
BH
CD
CH
BD
Vita9c Combined
g
Male
Variance percent
Vg
Vgxg
Ve
unexplained
h
Female
Variance percent
i
Male
Drug
Cohort
Site
male max = 14%
male max = 2.1%
male max = 43%
j
Female
White = 0–1%, faint = 1–2%, light = 2–4%, medium 4–8%, strong 8–16%, dark 16–32%, darkest 32–43%
Drug
Cohort
Site
female max = 28%
female max = 2.1%
female max = 24%
Suvivorship T-age (d)

Fig. 2 | Dynamics of *Vita* loci, their contributions to heritability, and source of variance. a–f, Genetic effect plots define changes across survivorships for the four genotypes at six diverse types of *Vita* loci. The relative effects of genotypes in days are marked by colored lines in days of difference from the average on the y-axis. The two-letter labels define genotypes**.** LOD scores are plotted along the bottom of each plot as a black trace above the T-age x-axis. *Vita* locus names and the sex are marked in all panels. **a,** *Vita1b* has durable and relatively uniform actuarial effects that extend from T_{42} to T_{900} survivorships. The initially negative effect of the *BD* genotype in most survivorships is caused by high late mortality starting at T_{855} (*Results* for explanation). **b,** Vita*14b* is a candidate rate of aging modulator (RAM) in males that has its highest LOD scores in the male survivorships at T_{42} that reflects a life-long and uniform *BD* versus *CH* contrast in mortality rates. **c**, *Vita1c* has early effects in male mortality from the infections at T_{365} and T_{590}. **d,** The significance of the *Vita2c* LOD score in mid survivorships is an artifact of sex-combined data and can only be understood in the context of major sex differences at this locus in both early and late survivorships (Extended Data Fig. 1f). **e,** *Vita4a* has striking reversals of effects between T_{450} and T_{780} due to offset waves of mortality in *CH* males and later in *BD* males. The *CH* genotype has a third derivative of roughly +0.00004 days/day³ around T_{605}, the peak rate of change of mortality rates (i.e., its acceleration). This positive value captures the inflection point at which the downward trend begins to decelerate before eventually reversing. **f**, *Vita9c* is an example of a locus with actuarial effects after T_{935} that are due to complex sex difference (Extended Data Fig. 1q). **g,h,** Comparison of the variance explained across all survivorships specifically by peak markers. The pink boxplots (*Vg*) are estimates of variance that can be explained by all 29 *Vita* loci. The blue boxplots are similar estimates of variance explained by the specific sets of significant epistatic interactions (*Vgxg*) defined in Fig. 4b. The green boxplots (*Ve*) estimate the summed environmental and experimental variance further broken down in panels **i** and **j**. The orange lines are smoothed averages of the variance that we cannot explain, including gene-by-environmental effects and higher-order genetic factors such as indirect genetics effects of cage mates. **h,** female components as above, but note significantly lower values, although the y-axis scale is the same. The gray horizontal lines at 10% and 37.5% in (**g**) and (**h**) are to help compare levels of variance between sexes. **i,j,** Breakdowns of experimental sources of variance. Rows labeled *Drug* are variance estimates of dietary interventions compared to control diet. *Cohort* is variance associated with birth cohort year—nine total. *Site* is variance attributable to differences at the three vivaria. For a display of *Vg* of individual *Vita* loci at all survivorships see Extended Data Fig. 3.

2. **Loci with steadily diminishing actuarial effects** that we refer to as rate of aging modulators (RAMs). These loci are characterized by uniform genetic effects on mortality rates that is visible as a contrast in mortality rates between at least two genotypes that starts at 200 day and extends to at least the T_{750} survivorship in one or both sexes. In table 1 we list 14 RAMs using a liberal definition of "relatively uniform", but half would be accepted at the higher stringency of an almost age-independent mortality rate difference. Most RAMs have effect sizes that converge toward 0-day differences in terminal survivorships. Among the latter are *Vita2b* in females, *Vita11c* in males, *Vita14b* in both sexes, and *Vita17a* and *VitaXa* in males (Fig. 3f, Extended Data Figs. 1x, 2x). *Vita14b* (Fig. 2b) and *Vita17a* are two example in which the initially high survivorship difference between *CH* and *BD* genotypes fades smoothly from T_{305} to T_{1100} in males (Extended Data Figs 1aa, 2aa).

3. **Loci with age-range restricted effects.** This category includes loci with action limited to early, middle, or late survivorships (Fig. 2c-f):

   a. **Early-age loci have strongest effects before T_{500}**. The 15 loci of this type are more than three times as common in males than females (Table 1). The best examples are *Vita6a* (Fig. 2c), *Vita1c*, *Vita1d*, *Vita2a* (Extended Data Figs 1c, 2c2), and *Vita18a* (Extended Data Figs 1ab, 2ab). For example, the 50-day spread in mortality risk of carriers of the four genotypes at *Vita1c* (Fig. 2c) is restricted to males (Extended Figs. 1c, 2c1, 2c2). Exceptions are notable because polarities of genotype effects are flipped between sexes at three of these loci—*Vita9a*, *Vita11b*, and *Vita18a* (Extended Data Figs 1n,s,ab, 2n1,s1, ab1). Only *Vita13*a has effect polarities shared by both sexes

(Extended Data Figs 1v, 2v1). The male bias in this type of locus is linked to higher mortality rates in T_{200} to T_{700} survivorships (Fig.1a,b).

b. **Mid-survivorship loci have strong effects from T_{500} to T_{845}.** There are six loci of this type. Examples include *Vita12a* and *Vita2c* (Fig. 2c,d). *Vita4a* is impressive because there is a strong biphasic fluctuation in the mortality rate of *BD* and *CH* genotype classes restricted the T_{500} to T_{710} interval in male survivorships (Fig. 2e, Extended Data Figs 1i, 2i1, 2i2). The effect is due to a 180-day offset in the start of two waves of mortality—the first at T_{230} caused by differences between *C* and *B* effects, the second at T_{410} caused by differences between *H* and *D* effects. The temporal offset in these waves is more obvious in the haplotype effect plots that complement the genotype effect plots (Extended Fig. 2i1 versus Extended Fig. 2i2).

c. **Late-acting *Vita* loci have effects after T_{860}.** Five loci have their main effects after T_{845}. *Vita9b* and *Vita9c* have very late effects (e.g., Fig. 2f, Extended Data Fig 2o2) and *Vita5a* acts with most force only in male survivorships after T_{730} (Extended Data Fig. 1k). This category could include loci such as *Vita1a* that have strong late-life effects on mortality, but we do not include them for actuarial reasons. *Vita1a* predicts lifespan soon after birth, while the formally defined late-acting class of loci have no actuarial impact until the oldest survivorships.

4. **Loci with reversals of genetic effects.** Twelve loci have genotype effects that reverse across survivorships. Reversals can involve a single genotype (the red *BD* trace in Fig. 2a) or two or more, for example *BD* and *CH* effects of *Vita4a* in males (Fig. 2e).

Dynamics of heritability

The cumulative variance explained by all 29 *Vita* loci on lifespan is higher in males than females from T_{42} to T_{320} (Fig. 2g,h) but drops from its base at 40% to 30% by T_{500} (Fig. 2g, Extended Data Fig. 3). The decline is due to a wave of early male mortality. By T_{650} male heritability has rebounded and it continues to climb to 50% in the oldest survivorships. Female heritability is almost precisely 27% in all survivorships up to T_{620} but then drops to 20% by T_{890}—450 days after the male low point. Like males, female heritability also recovers in the oldest survivorships, although still 10% lower than that of males. One important refinement: the variance we can explain by epistatic interactions between *Vita* loci (V_{gxg} in Fig. 2g,h) is twice as high in females as in males—12% versus 6% over the entire reproductive life.

We estimated the impact of three important non-genetic sources of variance: 1. treatment with or without a nominally ineffective dietary agent, 2. the cohort year of birth, and 3. environmental differences at the three sites. Collectively, these factors differ significantly between sexes in magnitude and in their age-dependence (Fig. 2g,h). The level is ~10% higher in males than females during the reproductive phase up to T_{605}. In males

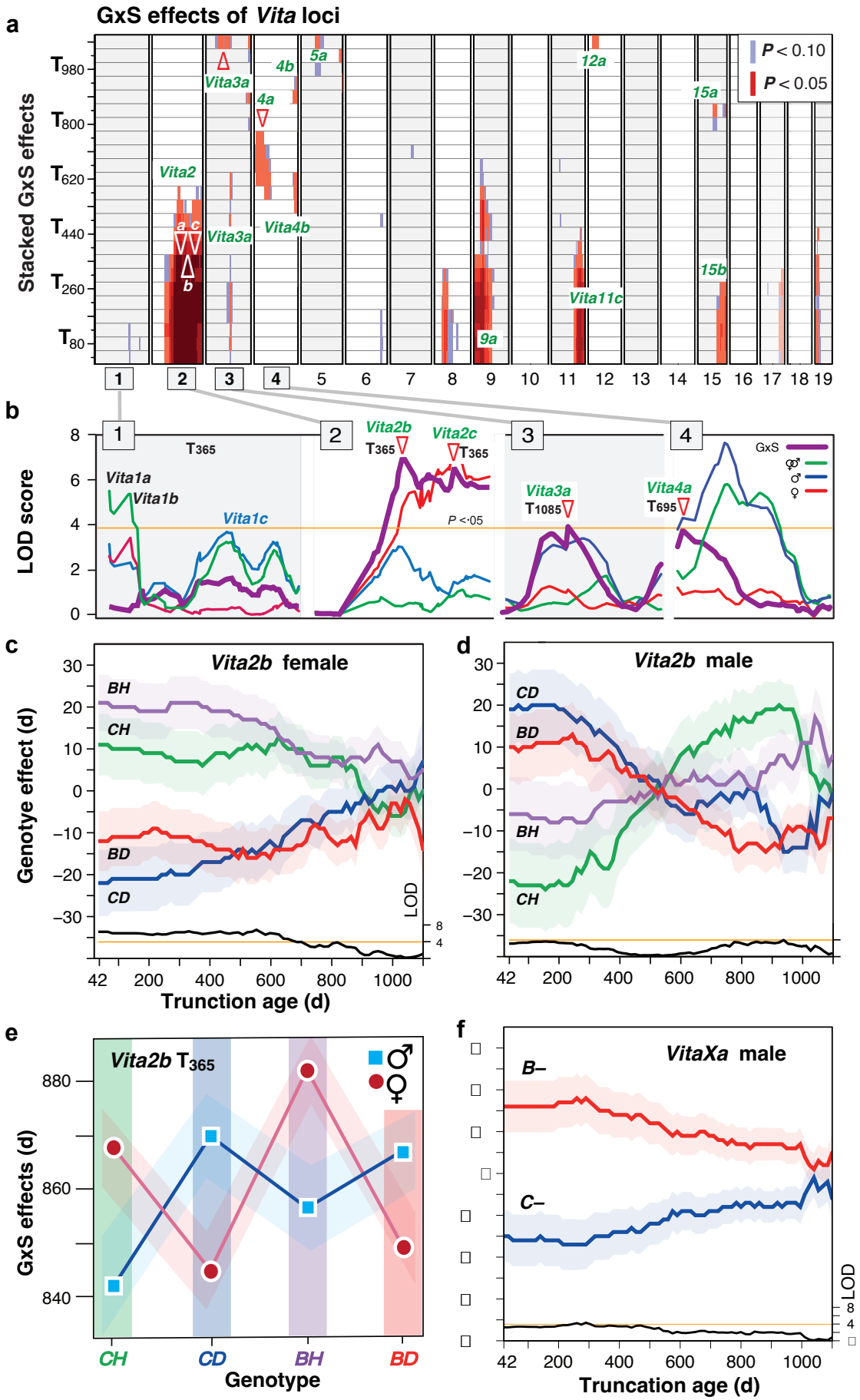
a
GxS effects of Vita loci
Stacked GxS effects
P < 0.10
P < 0.05
Vita3a
4b
5a
12a
15a
4a
Vita2
Vita4b
Vita3a
15b
Vita11c
9a
b
LOD score
Vita1a
Vita1b
Vita1c
Vita2b
Vita2c
Vita3a
Vita4a
GxS
P <·05
c
Vita2b female
Genotye effect (d)
BH
CH
BD
CD
LOD
Trunction age (d)
d
Vita2b male
e
Vita2b T365
GxS effects (d)
CH
CD
BH
BD
Genotype
f
VitaXa male
B–
C–
LOD
Truncation age (d)

Fig. 3 | Antagonistic sex effects within *Vita* loci. a, Overview of all significant (red) and suggestive (light blue) locus-by-sex interaction effects (GxS) across all *Vita* loci in all survivorships. The GxS effect on Chr 8 is most likely a real interaction of a locus that has a main effect below our threshold. The GxS values in Table 1 are more discrete and only test top markers in the most significant survivorship. **b**, The first four chromosomes illustrate the range of sex differences in effects of *Vita* loci at T_{365}. Red and blue lines signify female and male additive genetic effects, respectively (LOD scores), whereas the thicker purple lines signify the GxS effect, and the green lines are the "unsexed" or combined additive effect. Orange line is the genome-wide significance threshold at LOD 3.95. There are no GxS effects on Chr 1 (**b**, left). *Vita* loci with significant GxS on chromosomes 2, 3, and 4 are highlighted in green with the truncation age of maximal GxS interaction at the location of the red triangles. **c** and **d**, *Vita2b* effect plots demonstrate how sex-averaged data obscures effects: while the additive effects are significant before T_{700} in females (**c**) they are only significant after T_{700} in males (**d**). **c** and **d** highlight the antagonism of sex effects of the four genotypes, and reversals of all effects in males at T_{515}. **e**, The GxS difference and standard error of lifespans of males and females for the four genotypes. At T_{365} the C*H* and *BH* genotypes are advantageous for expectancies of females and the *CD* and *BD* haplotype for males. **f**, In males the hemizygous *B* haplotype at *VitaXa* has a 30-day positive effect on lifespan compared to *C* at T_{42}, with a gradual decline in effect size typical of a RAM-type locus. The decline—or convergence—from the T_{305} survivorship onward is due to a higher proportional *C* haplotype mortality.

the level peaks at 53% at T_{440} but then drops in rough synchrony with andropause[46–48]. Less than 20% of variance in older survivorships of both sexes is linked to these non-genetic sources—a counter-intuitive reduction in sensitivity to exogenous factors later in life. The remaining unexplained sources of variance (orange lines in Fig. 2g,h) include uncontrolled environmental and technical factors, including data errors, higher order interaction effects that we have not modeled, and indirect social genetic effects[49].

We decomposed variance components associated with these three variables: 1. drug supplement, 2. cohort year, and 3. site (Fig. 2i,j). Despite intense efforts to standardize protocols, variance attributable to sites is up to 43% in males and 24% in females. In males the variance associated with receiving a supplement versus control diet was much more modest than site (Fig. 2i) although the supplement still increased lifespan by 40.2 ± 8.3 SE days at T_{42}. In contrast, in females the effect of supplements was greater than that of site (Fig. 2j) and increased lifespan by 37 ± 6.7 SE days. The positive drug effect persists to T_{680} in males and to T_{800} in females (Fig. 2i) but turns negative by T_{890} in males (–11.7 ± 5.3 SE days, $P = .03$) and by T_{1040} in females (–10.2 ± 5.3 SE days, $P = .06$). Cohort year is not a significant source of variance in either sex.

Vita loci have strong and antagonistic sex interactions

Males have an 80-day lower life expectancy than females at T_{42} (Fig. 1b, $P < .0001$) that can be decomposed into sets of loci, including those that specifically influence GxS interactions (Fig. 3a,b). The likely proximal cause is higher aggression and stress among co-housed males[50–53]. The high mortality is visible in effect plots for *Vita1c*, *Vita2a*, and *Vita6b* (Fig. 2d, Extended Data Figs 1, 2) and for *Vita2b* (Fig. 3c,d). All loci have strong but transient effects. As a result, the male disadvantage is eliminated in survivorships above T_{725} (Fig. 1b). In survivorships from T_{935} to T_{1100} males typically are housed solo and gain a small 8-day advantage over females (T_{1040}, $P < .036$). While studies of sex differences in longevity of mice have had mixed results[54], there are unequivocal age-dependent sex differences in life expectancies in both wild[55] and laboratory populations. Higher mortality of younger males creates a downstream ascertainment bias in older survivorships, and living alone in old age is a serious environmental perturbation. Both may paradoxically contribute to the small but significant life expectancy advantage of males in older survivorships. Sex differences in lifespan of humans

have a different pattern: men consistently have 1.25 to 1.46-fold higher mortality rates than women in elderly cohorts without any convergence even by 100 years[56].

Fourteen *Vita* loci have strong gene-by-sex (GxS) interaction effects (Table 1, Fig. 3a). The complex of loci on Chr 2 is an extreme example (Fig. 3a-d). *CH* and *BH* genotypes at *Vita2b* are advantageous to females until T_{700} (Fig. 3e) but are disadvantageous to males until only T_{365}. Polarities of the strong sex effects of *CD* and *BD* genotypes are also reversed (Fig. 3e). This sex reversal fades by T_{545} (Fig. 3d). *Vita2b* has a massive GxS effect with a LOD of 8.6 at T_{140} that is lost entirely by T_{800} (Fig.3a). The effect has features associated with antagonistic pleiotropy in males (Fig. 3c,d) in the sense that polarities reverse in $T_{450–545}$ survivorships.

Vita2a, Vita2b, and *Vita2c* are cautionary examples of how mapping both sexes together without including an interaction term can mislead. A sex-combined analysis defines a highly significant peak at T_{800} for *Vita2c* and *Vita2b* (Fig. 2d, Fig. 3c,d) that is an artifact of not fitting the interaction (Extended Data Fig. 1e,f). GxS mapping unmasks two independent interactions at the extreme distal end of Chr 4 (154 Mb) at the "male-only" *Vita4b* locus: one at T_{605}, the other at T_{905} (Fig. 3a). The male-specific *VitaXa* locus maps to proximal Chr X (Fig. 3f). The *B* haplotype confers an initial 30-day benefit compared to *C*, but this effect diminishes steadily toward death as expected of a RAM-type locus. In contrast, in heterozygous females the segregating *C* and *B* haplotypes do not differ at all or in any survivorships (Extended Data Figs 1ac, 2ac).

Epistatic interactions between *Vita* loci are sex- and age-specific

We detected epistatic interactions among *Vita* loci in both sexes at T_{42}, T_{365}, T_{740}, and T_{905}. There are 41 interactions among 359 non-syntenic pairs of loci at T_{42}: 19 in females and 22 in males with LODs ≥3.8 (Fig. 4a,b, Table 1). The strongest male interaction is between *Vita1c* and *Vita3a* (Fig. 4d, LOD 5.0). Effects of *BD* and *CH* genotypes at *Vita3a* across the four *Vita1c* genotypes produce remarkable lifespan swings of up to 100 days (Fig. 4d), but the interactions are lost by T_{740} (Fig. 4f).

The strongest female interactions are those between *Vita1c–Vita2b*, *Vita1b–Vita9a*, and *Vita3a–Vita5a* (Fig 4c,e,h). The *BD* genotype at *Vita1b* masks *any* effects of *Vita9a*—the classic Mendelian definition of epistasis (Fig. 4e)[57]. This interaction fades by T_{905} (Fig. 4g). Other interactions are durable at least to T_{740}, and in these older survivorship can be shared by both sexes, for example, the *Vita1c–Vita2b* pair (Fig. 4h). The polarities of epistatic interactions can display sexual antagonism[58–61], particularly those of the *Vita2b CD* genotype (blue line) across *Vita1c* genotypes (Fig. 4c). *Vita1c* does not have any main effect in females or any GxS effects (Table 1, Fig. 1e, Fig. 3a), but exposes a forceful and surprising interaction with *Vita2b*[62].

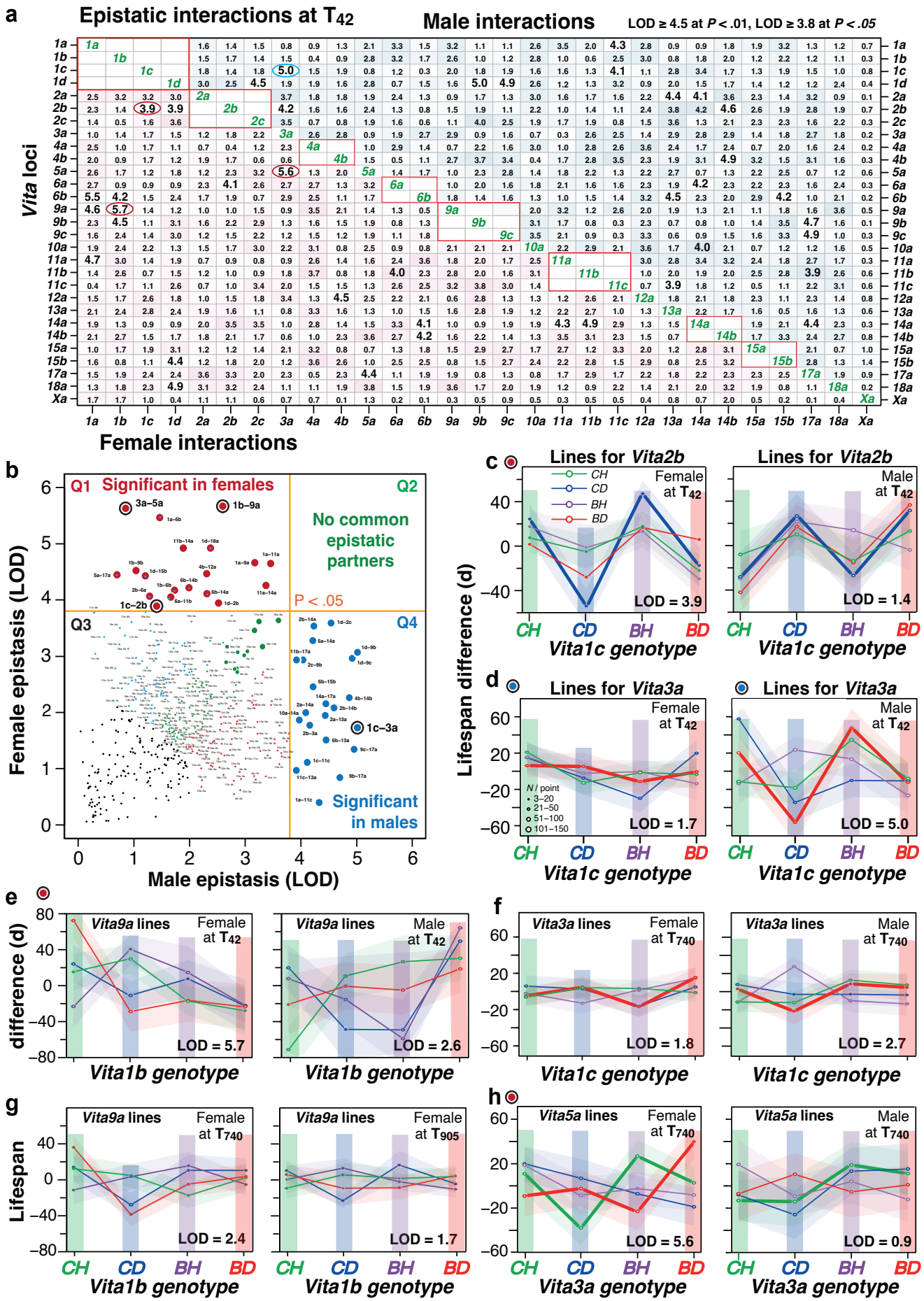
a
Epistatic interactions at T42
Male interactions
LOD ≥ 4.5 at P < .01, LOD ≥ 3.8 at P < .05
Vita loci
Female interactions
b
Q1 Significant in females
Q2
No common epistatic partners
Q3
Q4
P < .05
Significant in males
Female epistasis (LOD)
Male epistasis (LOD)
c
Lines for Vita2b
Female at T42
Male at T42
CH
CD
BH
BD
LOD = 3.9
LOD = 1.4
Vita1c genotype
Lifespan difference (d)
d
Lines for Vita3a
LOD = 1.7
LOD = 5.0
N / point
3–20
21–50
51–100
101–150
e
Vita9a lines
LOD = 5.7
LOD = 2.6
Vita1b genotype
f
Vita3a lines
T740
LOD = 1.8
LOD = 2.7
g
Lifespan
T905
LOD = 2.4
LOD = 1.7
h
Vita5a lines
LOD = 5.6
LOD = 0.9
Vita3a genotype

Fig. 4. Epistasis among *Vita* loci. a, A full matrix of with LOD scores of the locus-by-locus interactions in the T_{42} survivorship of all animals in which the upper triangular matrix tabulates male scores, the lower tabulates female scores. LODs at or above 3.8 in large font. There is minimal commonality between male and female epistasis. Similar matrices are given for all four ages for three sex combinations—combined, females only, and males only in Supplementary Table 12. **b,** Correlation plot of female versus male epistasis in the T_{42} survivorship. Those above threshold are marked in red for females (*N* = 19), in blue for males (*N* = 21) and labeled by *Vita* pair numbers. There are no points significant LODs shared by both sexes in quadrant Q2. However, the green points in Q3 highlight some low-level epistatic interactions shared by both sexes. The rho correlation of male and female LOD scores is 0.32. **c,** A pair of effect size plots of a strong female epistatic interaction between *Vita1c* and *Vita2b* at T_{42} that is also highlighted with a bullseye in **b**. The colored columns define the four genotypes at the first locus (*Vita1c*) whereas the four colored lines define genotypes of the second locus (*Vita2b*). The y axis is the lifespan difference of the 16 points in each panel. Compare the polarity of female and male effects of the *CD* genotype (thicker blue lines)—an example of modest antagonistic epistasis between *sexes*. **d,** One of the highest male interactions is between *Vita1c* and *Vita3a*, highlighted by the blue bullseye in (**b**). There is no interaction in females (left). **e,g,** A quartet of epistatic interactions at T_{42}, T_{740}, and T_{905}. The *Vita1b*–*Vita9a* interaction is the highest we have detected in females (**e**) with a classic masking effect of the *BD Vita1b* genotype in which all lines converge in the pink *BD* column. The male pattern is different and not significant (**e**, right). **g,** The strong *Vita1b*-*Vita9a* interaction steps down in females at T_{440} and at T_{905}. **h,** The *Vita3a*-*Vita5a* interaction is weak in young females (0.9 in (**a**)) but very strong in females at T_{740}. Point sizes vary as a function of numbers of individuals per genotype pair. Almost all points are well above *n* of 50.

Epistatic interactions at T_{42} are unique to one or the other sex, and for this reason, quadrant 2 is empty (Q2 of Fig.4b). Even those loci with minimal sex differences do not share partnerships (Fig. 4a). *Vita1b* pairs with *Vita6b*, *Vita9a*, and *Vita9b* with LODs of 4.2, 5.8, and 4.5 in females, but in males the corresponding LODs are 1.5, 2.6, and 1.1. This marked difference is consistent with antagonistic epistasis between the sexes[63,64,65]. We estimated variance of the full sets of interactions in Q1 and Q4 across all T-ages (Fig. 2g,h). In females the variance peak is 12% at T_{42} but drop to 1.6% by T_{995} (Fig. 2h). In males the peak is 6.8% at T_{42} but drops to 1.4% by T_{905} (Fig. 2g).

Soma loci direct trade-offs between body weight and lifespan

Mice were weighed at 42, 183, 365, 548, and 730 days. Weights at 42, 183, and 365 days correlate negatively with subsequent lifespans in both sexes (Fig. 5e) as expected from previous work[66,67]. These rank order correlations are stronger in males than females—a rho at T_{185} of –0.28 versus –0.11 ($P < .001$)[68]. This translates to a loss of about 14.3 days per gram in males but only 3.7 d/g in females (Fig. 5e,i,j). Sex differences are significant from T_{185} to T_{800} (bold linkage score trace in Fig. 5e, $P < .05$, FDR at –log*P* of 1.64). Correlations in females are stable throughout adulthood with values close to –0.1 (Fig. 5e-h). In contrast, the negative correlation in males erodes with age and overlaps female values in older survivorships (T_{900}, Fig. 5f-h). Correlations of weight and life expectancy become positive in both sexes after 730 days (Fig. 5h). We mapped body weights acquired at all five ages (±5 days) and detected 28 *Mass* loci that we subsequently used to compare with the *Soma* loci described below (Fig. 5a-c, Extended Data Fig. 4).

To identify genetic causes of both negative and positive weight-to-lifespan relations we mapped genotype-specific differences in rank order correlations at all five ages across all applicable (later) survivorships—five full actuarial scans in 15-day steps. We defined 30 *Soma* loci (Table 2, Fig. 5b,c, Extended Data Fig. 5) at which rho differs significantly by genotype at one of the five specific T-ages when weights were obtained (e.g., weight at 548 days tested at T_{550}). Only seven of these *Soma* loci overlap body weight *Mass* loci—a frequency expected by chance ($P = 0.28$, Fig. 5a vs. Fig. 5b,c, and Extended Data Fig. 5). Fifteen are detected

									Soma Positions (Mb, GRCm38) ¥					Days Gained or Lost per Gram at High T-Age ◊				Correlation of Weight with Lifespan (rho) ◊				*Mass* Overlap		*Vita* Overlap		
	Locus	Max. –Log*P* Any T-age @	–Log*P* When Weighed †	High T-Age §	Sex Effects*	Effect Range (d/g)	Max. –Log*P* Any T-age †	Actuarial Range (d) Δ	Chr	Prox	Peak	Distal	Size	*CH*	*BH*	*CD*	*BD*	*CH*	*BH*	*CD*	*BD*	*Mass* Locus Overlap §	*Mass* Locus Type and Sex §	*Vita* Locus Overlap §	Locus Type and Sex §	Extend Data Fig. 3
1	***Soma1a***	3.95	3.42	185	C	8.3	4.0	≤365	1	0.0	3.0	24.0	24.0	-10.2	-11.8	-3.5	-4.5	-0.23	-0.26	-0.09	-0.12			***Vita1a***, *1b*	Durable (C)	a
2	***Soma1b***	4.09	3.85	730	M	4.3	4.1	≥730	1	63.9	86.2	133.6	69.7	5.1	1.4	0.9	5.2	0.32	0.07	0.08	0.32	*Mass1b*	Early (M)	*Vita1c*	Early (M)	b
3	***Soma2a***	3.56	3.50	185	M, C	10.4	3.6	≥183	2	0.0	13.6	24.6	24.6	-11.4	-21.8	-14.4	-16.1	-0.22	-0.43	-0.29	-0.38	***Mass2a***	Early (C)			c
4	***Soma2b***	5.07	3.12	42	C	47.4	5.1	≤548	2	30.4	60.2	83.9	53.5	7.3	2.7	-40.1	-30.2	0.07	0.03	-0.23	-0.23					d
5	***Soma2c***	5.09	2.77	42	M	30.8	5.1	42	2	148.4	161.9	180.1	31.6	-13.9	-13.1	-5.8	-36.6	-0.09	-0.09	-0.05	-0.34			*Vita2c*	Mid (F,M)	e
6	***Soma3a***	3.53	2.76	550	M	5.5	3.5	42, ≥548	3	42.2	88.0	108.2	66.0	1.3	-1.0	-3.7	-4.2	0.03	-0.05	-0.12	-0.17	***Mass3a***	Durable (C)	***Vita3a***	Early, Late (M)	f
7	***Soma3b***	4.93	3.95	185	M	9.5	4.9	All	3	121.5	159.6	159.6	38.1	-8.4	-13.7	-17.9	-16.7	-0.18	-0.29	-0.38	-0.34					g
8	***Soma4a***	4.02	3.32	42	M	20.0	4.0	All	4	0.0	11.2	30.8	30.8	-15.5	-31.9	-14.1	-34.1	-0.13	-0.28	-0.11	-0.22	*Mass4a*	Early (M)			h
9	***Soma4b***	3.55	3.15	42	C, M, F	20.4	3.6	≤183, ≥730	4	66.8	107.4	156.0	89.2	-12.9	-25.1	-4.7	-18.6	-0.13	-0.17	-0.02	-0.18	*Mass4b*	Durable (M)	*Vita4b*	Mid (M)	i
10	***Soma6a***	3.99	3.60	550	C, F	3.1	4.0	All	5	0.0	8.0	25.9	25.9	-2.9	-2.4	0.2	0.1	-0.15	-0.13	0.00	0.01					j
11	***Soma6b***	3.46	3.13	730	F	4.0	3.5	≥730	6	66.8	138.7	139.6	72.8	-2.2	0.3	0.4	1.8	-0.17	0.02	0.04	0.12			***Vita6b***	Early (M)	k
12	***Soma7a***	5.27	4.75	365	M	7.6	5.3	≥183	7	4.3	16.1	43.5	39.2	-14.5	-6.9	-10.2	-7.0	-0.38	-0.20	-0.26	-0.15					l
13	***Soma7b***	3.84	3.79	550	M	7.5	3.8	≥183	7	85.1	120.1	145.3	60.2	-2.0	-4.9	2.6	-4.8	-0.09	-0.17	0.06	-0.17					m
14	***Soma8a***	3.07	2.92	365	M	6.9	3.1	≤365	8	41.1	71.7	86.0	44.9	-8.3	-5.3	-12.2	-10.4	-0.22	-0.12	-0.33	-0.27					n
15	***Soma8b***	3.48	3.13	42	C	22.9	3.5	All	8	86.0	111.3	129.1	43.1	-11.9	-13.9	-28.5	-5.6	-0.11	-0.11	-0.25	-0.03					o
16	***Soma9a***	2.93	2.92	185	C	6.6	2.9	183	9	20.0	51.1	58.1	38.1	-13.0	-6.4	-10.0	-9.0	-0.30	-0.17	-0.23	-0.22			*Vita9a*	Early (F)	p
17	***Soma10a***	4.49	3.85	185	C,M	7.1	4.5	≤183, ≥730	10	0.0	18.1	90.1	90.1	-9.8	-9.0	-3.8	-10.9	-0.25	-0.22	-0.09	-0.25	*Mass10a*	Early (M)	*Vita10a*	Late (M)	q
18	***Soma11a***	4.22	3.31	365	F	3.6	4.2	All	11	50.4	97.4	113.7	63.3	-0.1	-3.7	-2.3	-2.0	0.03	-0.18	-0.15	-0.10	***Mass11c***	Durable (M)	*Vita11b*	Late (F)	r
19	***Soma12a***	3.88	2.97	185	F	6.1	3.9	183	12	58.3	71.7	79.1	20.8	-1.2	-7.3	-4.5	-2.8	-0.05	-0.24	-0.16	-0.08	***Mass12a***	Durable (F)			s
20	***Soma12b***	2.91	2.91	730	M	4.2	2.9	≥183	12	79.1	118.2	118.2	39.1	4.8	3.6	0.6	2.1	0.26	0.28	0.03	0.13			***Vita12a***	Mid (C)	t
21	***Soma13a***	3.52	2.80	42	M	46.0	3.5	≤183	13	4.4	19.4	67.3	62.9	12.3	-33.7	-25.1	-21.2	0.04	-0.28	-0.17	-0.21					u
22	***Soma13b***	4.71	3.22	42	F	25.0	4.7	42	13	77.3	98.5	111.4	34.1	-1.5	-22.3	2.7	-19.3	-0.06	-0.25	0.01	-0.11			*Vita13a*	Early (F M)	v
23	***Soma14a***	3.12	3.12	550	M	7.1	3.1	183 – 548	14	20.7	31.0	31.0	10.3	-0.1	-4.7	-0.8	2.4	-0.02	-0.17	-0.06	0.07					w
24	***Soma14b***	3.89	3.88	42	M	49.7	3.9	42	14	79.4	101.4	120.3	40.9	-45.8	-6.9	3.9	-18.1	-0.35	-0.07	0.06	-0.12	***Mass14a***	Early (C)	***Vita14a***	Early Mid (C)	x
25	***Soma15a***	4.50	4.34	185	M	16.4	4.5	183 – 548	15	0.0	3.3	20.7	20.7	-7.1	-3.6	-20.0	-13.5	-0.15	-0.09	-0.43	-0.31					y
26	***Soma16a***	3.86	2.76	550	C, F	4.3	3.9	≥548	16	38.0	75.8	96.4	58.4	-5.1	-4.8	-9.1	-8.4	-0.15	-0.13	-0.26	-0.22	***Mass16a***	Early Mid (M)			z
27	***Soma17a***	2.97	2.87	730	F, C	2.6	3.0	183F, 548M, 730F	17	0.0	26.5	68.8	68.8	-0.8	-1.1	1.5	1.1	-0.06	-0.09	0.14	0.09	*Mass17a*	Time Diff (MF)	***Vita17a***	Durable (M)	aa
28	***Soma18a***	4.68	3.30	42	C	24.0	4.7	42M, 42–365F	18	21.1	52.5	70.8	49.8	-0.9	-13.2	-24.9	-14.5	0.02	-0.10	-0.24	-0.16			***Vita18a***		ab
29	***Soma19a***	3.32	3.32	730	M	4.4	3.3	730	19	0.0	3.4	11.6	11.6	4.1	-0.3	3.9	3.2	0.27	-0.02	0.21	0.21					ac
30	***Soma19b***	3.00	3.00	730	M	5.1	3.0	730	19	35.0	53.9	62.0	27.0	4.3	-0.8	3.0	2.8	0.23	-0.04	0.22	0.18	***Mass19a***	Early Mid (M)			ad

@ **Max –LogP Any T-age** is the maximum value across any actuarial scan from any of the five ages at which mice were weighed. This value was **not** used to establish significance.

† **High –LogP When Weighed** is the highest –logP corresponding to one of the five ages at which mice were weighed. This value is genome-wide significant at P < .05 with BH correction at values ≥2.75.

§ **High T-Age** is the T-age at which mice were weighed that gave the **High–Log*P* When Weighed** *value*. If the **High T-age** is 730, then all values correspond to the T730 surviorship for the first listed **Sex Effects**.

* **Sex Effects** where **C** = combined, **F** = female, and **M** = male given in the order corresponding to data for **High –LogP** and **HIgh T- Age**.

Δ **Actuarial Range** in days associated with *Soma* loci. When two age ranges are given they apply in order of **Sex Effect**s. Soma15a

¥ ***Soma*** chromosomes **(Chr)** and **Positions** using GRCm38 coordinates. **Prox** and **Distal** are proximal and distal marker positions. **Size** of locus in **Mb** (megabases).

◊ Effects sizes for genotypes at the **High T-Age** and first **Sex Effects** group. Green, blue, beige shading for combined, male, or female data.

§ ***Mass*** **Locus Overlap** and ***Vita*** **Locus Overlap** with the *Soma* locus. If **bold** then peaks are within 10 Mb. **Vita Type and Sex** from Table 1, abbreviated.

◊ **Days Gained or Lost** effects sizes for ***CH***, **BH**, ***CD***, and ***BD***)genotypes at the **High T-Age** for first **Sex Effects** group. Similar values for **Correlation of Weight**. Green, blue, beige shading for combined, male, or female data.

only in males; four only in females (Table 2). Nineteen *Soma* loci have significant genetic variation in negative correlations using weights acquired at 42 and 185 days. Eleven have significant genetic variation in positive correlations when using weights acquired at older ages (Table 2).

The effects of *Soma* loci on lifespan range from 2 d/g to 29 d/g at T_{42}, T_{185}, T_{365}, T_{730} days (colored columns in Table 2). We highlight *Soma3b* that has strong effects in males (Fig. 5i) but none in females (Fig. 5j). Males with the *CD* genotype lose 17.9 d/g; those that inherit *CH* only lose 8.4 d/g. In females, differences of negative correlations are insignificant (*CH:* –2.9 d/g versus *CD:* –3.4 d/g). *Soma11a* has the strongest impact on females (Table 2, Extended Data Fig. 5), but even its effects—6 d/g between *CH* and *BH* genotypes—are modest. *Soma* loci overlap *Vita* and *Mass* loci (Table 2) at chance level. The summed genome-wide coverage of *Soma* loci is 1349 Mb, 48% of the mouse genome[69]; that of *Vita* loci is 1000 Mb (36%). Seven *Soma* loci have peaks within 10 Mb of *Vita* peaks, also insignificant (P = .19). However, two pairs do share the same position, the same survivorship ages, and the same sex bias, and perhaps the same causal DNA variants. *Soma3a* and *Vita3a* have peaks within 4 Mb and modulate male longevity early and late in life. *Vita1a* and *Soma1a* share top markers in both sexes, but the *Soma* effect is limited to weight at 365 days whereas the mechanistic effect of *Vita1a* does not manifest itself until after T_{900} (Fig. 1f). *Vita1a* and *Soma1a* are modulated by the *H* and *D* haplotypes (Fig. 1f, Extended Data Fig. 2a Extended Data Fig. 5a). *H* lengthens life by 12 days, while *D* shortens life by 22 days. This effect is shared by both sexes (combined LOD = 6.5). Genetic effects of *Soma1a* oppose those of *Vita1a*, particularly in females. *H* decreases expectancy by –4 d/g (average rho of –0.12), whereas *D* increases expectancy by 1 d/g (rho of +0.02, Extended Data Fig. 5a). All effect plots, for example those in Fig.

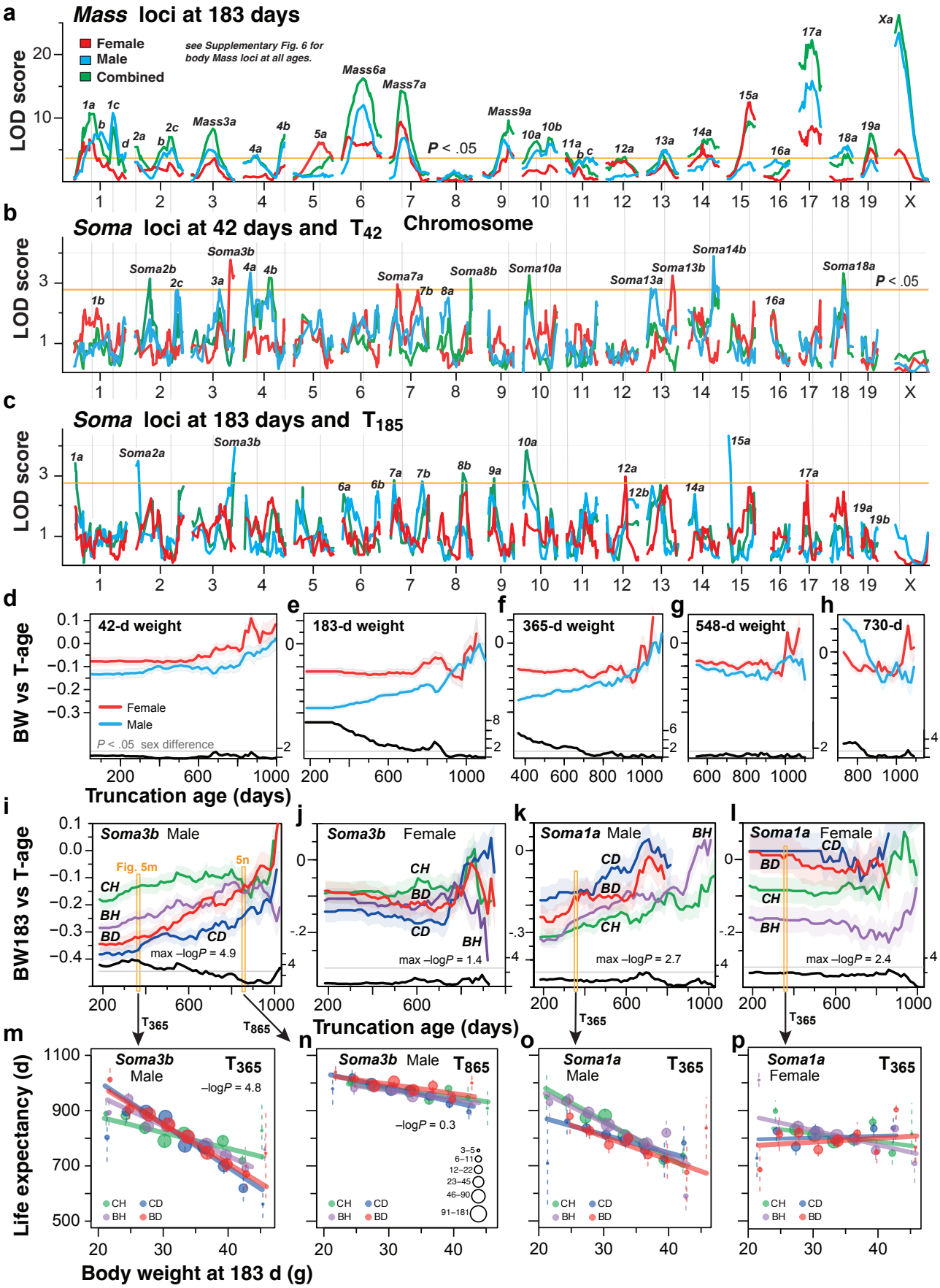
a
Mass loci at 183 days
Female
Male
Combined
see Supplementary Fig. 6 for body Mass loci at all ages.
LOD score
P < .05
Chromosome
b
Soma loci at 42 days and T42
c
Soma loci at 183 days and T185
d
42-d weight
e
183-d weight
f
365-d weight
g
548-d weight
h
730-d
BW vs T-age
P < .05 sex difference
Truncation age (days)
i
Soma3b Male
j
Soma3b Female
k
Soma1a Male
l
Soma1a Female
BW183 vs T-age
max −logP = 4.9
max −logP = 1.4
max −logP = 2.7
max −logP = 2.4
Fig. 5m
5n
T365
T865
m
n
o
p
Life expectancy (d)
−logP = 4.8
−logP = 0.3
Body weight at 183 d (g)

Fig. 5 | The genetic modulation of life expectancy by body weight is stronger in males than females. **a,** Conventional QTL maps of body mass (*Mass* loci) at 183 days for both sexes and combined. There are 25 significant *Mass* loci at T_{183} (see Extended Data Fig. 4 for all other ages). The yellow horizontal lines in **a**, **b** and **c** are genome-wide acceptance thresholds. The faint vertical gray lines at *Mass* peaks do not overlap significantly with *Soma* loci. **b,** Maps of the *Soma* loci that modulate correlations between body weight at 42 days and life expectancy in theT_{42} survivorship. Several loci are named despite being below threshold at this age or in (**c**). **c,** Corresponding *Soma* loci for body weight at 183 days (6 months) with life expectancy at T_{185}. **d-h,** Actuarial plots for correlations of body weight at five ages (42, 183, 385, 558, and 730 days) for males and females. In panel (**d**) there is only a modest correlation of weight at 42 days with subsequent lifespan in any survivorship in either sex, but by 183 days in (**e**) there is a strong negative correlation in males and a significant sex difference (–log*P* of the sex difference is given above the x-axis). **g,** There is no sex difference at 548 days. **h,** Body weight at 730 days has a positive correlation in males but by the T_{1040} survivorship the female correlations are higher. **i,j,** Actuarial plots of correlations between weight at 183 days with subsequent survivorships for *Soma3b* for males (**i**) and females (**j**). Correlations of the four color-coded genotypes differ significantly for males in the T_{365} survivorship (left orange bar) but not in the older T_{665} survivorship. The –logP *Soma* scores are given along the x-axis (black trace) with the maximum actuarial value. Note arrows from orange bars to panels (**m**) and (**n**)—cross-sectional views of these weight to life expectancy correlations at T_{365} that are highly significant in the T_{365} survivorship with a –logP of 4.8 but not significant in the T_{865} survivorship in (**n**). **k,l,** Comparison of survivorship differences between males and females at *Soma1a*. *Soma1a* is close to the significance threshold in males in the T_{710} survivorship. Orange bars correspond to **o** and **p**. LOD scores (black lines) above the x-axis are significant at 2.75. Note the y-axis scale differences between sexes. **m-n,** Plots of *Soma3b* correlations (Spearman rank rho) in males in T_{365} and T_{865} survivorships. Survivorships were binned in 2-gram weight classes. The six circles sizes provide approximate sample size per class scaled to the log of the number. **o,p,** Comparison of male and female sex differences in *Soma* correlations that correspond to panels **k** and **l** at T_{365}.

5i-l, are provided in Extended Data Fig. 5 for all loci, both sexes, and T-ages. These full actuarial scans have –log*P* peaks (Table 2) that are on average slightly higher (+0.5) than the level used to gauge genome-wide significance.

From maps to mechanisms

Most *Vita* loci are too large for resolution of causal DNA variants or mechanistic dissection of mortality rates. However, 19,000 more UM-HET3 mice are available for genotyping which already motivates a foray into mechanistic studies[22,38,70,71]. For each *Vita* locus we have assembled details on gene variants segregating in the UM-HET3 with predicted functional impact and roles in aging[72,73]. Here we highlight both limitations and prospects of analysis at this stage. The two largest loci almost certainly encompass many linked variants. *Vita17a* extends from the centromere to 74 Mb (Table 1), overlapping the major histocompatibility complex, known since the 1970s to be linked to lifespan[74,75]. *VitaXa* is detected only in males and covers the proximal 70 Mb of Chr X and is also an intractable oligogenic locus. Males with *B* haplotypes live 30 to 15 days longer than those with *C* haplotypes from T_{300} to T_{1010} (Fig. 3f)[76].

In contrast *Vita1a*, *Vita9b*, and *Vita15b* are much more tractable. *Vita1a* is compact, overlapping just 14 protein-coding genes of which *Atp6v1h*, *Rb1cca*, and *Mrpl15* are strong candidates involved in autophagy, nutrient sensing, and mitochondrial function[70]. *ATP6V1H* has ubiquitous activity as an modulator of vacuolar acidification[77]. It extends *Drosophila* lifespan[72,78], and modulates insulin secretion and type-2 diabetes risk[79]. *Atp6v1h* also harbors a 11.5 Kb repeat in intron 7 in the *D* haplotype[80]. The homozygous knockout mouse is lethal early in life (www.mousephenotype.org/data/genes/MGI:1914864). Our finding that *Vita1a* has strong epistasis with *Vita6b*, *Vita9a*, and *Vita11a* is a valuable constraint when evaluating gene candidacy using

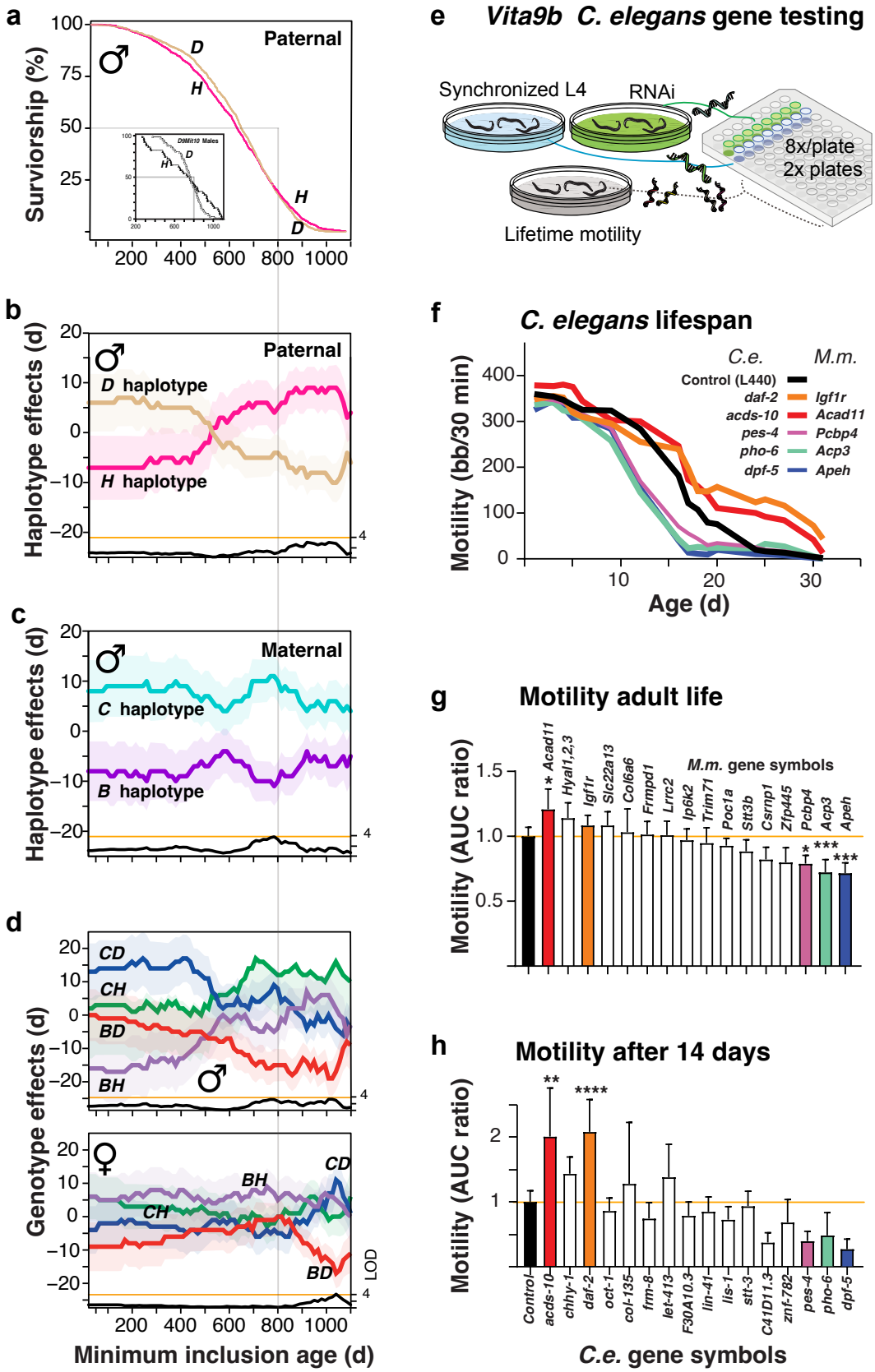
a
Paternal
Surviorship (%)
D
H
D9Mit10 Males
b
Paternal
Haplotype effects (d)
D haplotype
H haplotype
c
Maternal
C haplotype
B haplotype
d
Genotype effects (d)
CD
CH
BD
BH
LOD
Minimum inclusion age (d)
e
Vita9b C. elegans gene testing
Synchronized L4
RNAi
8x/plate
2x plates
Lifetime motility
f
C. elegans lifespan
Motility (bb/30 min)
Age (d)
C.e.
M.m.
Control (L440)
daf-2
acds-10
pes-4
pho-6
dpf-5
Igf1r
Acad11
Pcbp4
Acp3
Apeh
g
Motility adult life
Motility (AUC ratio)
M.m. gene symbols
Acad11
Hyal1,2,3
Igf1r
Slc22a13
Col6a6
Frmpd1
Lrrc2
Ip6k2
Trim71
Poc1a
Stt3b
Csrnp1
Zfp445
Pcbp4
Acp3
Apeh
h
Motility after 14 days
Motility (AUC ratio)
Control
acds-10
chhy-1
daf-2
oct-1
col-135
frm-8
let-413
F30A10.3
lin-41
lis-1
stt-3
C41D11.3
znf-782
pes-4
pho-6
dpf-5
C.e. gene symbols

Fig. 6 | Genetics of *Vita9b* and candidate gene analysis. **a,** Kaplan-Meier plot for paternal haplotypes in male UM-HET3 mice at *Vita9b*. The *D* haplotype has a survival advantage compared to the *H* haplotype until 800 days (faint vertical line through panels **a-e**). The small KM insert box is redrawn from Jackson et al. (2002) who detected the same effect at this locus in a separate cohort (*D9Mit10*). **b,c**, Contrasting effect plots for paternal (*H, D*) and maternal (*C, B*) haplotypes along with LOD scores. Life expectancies of both *H* and *D* haplotypes invert between T_{250} and T_{900}. Those of *C* and *B* haplotypes are durable. **d,** Corresponding genotype plots of males and females that are significant only in old survivorships. **e,** Design of the *C. elegans* motility assay in which RNAi were used to knock down expression of target transcripts with two levels of replication. **f.** Time course of age-related changes in motility of 6 of 15 lines—the control (black), and the *daf-2* positive control (orange). Effects of RNA knockdowns on motility of 15 orthologs of *Vita9b* candidates in *C. elegans*. **g,** Summary of motility over most of adult life (1 to 30 days). Asterisks are significant effects with correction for multiple tests. Of the 15 genes tested, 3 reduce motility significantly— *pes-4* (mouse *Pcbp4*), *pho-6* (*Acp3*), and *dpf-5* (*Apeh*). acds-10, an ortholog of the mouse *Acad11* gene, improves motility relative to control and in a pattern like that of *daf-2*. **h,** Motility after 14 days of age. Only effects of *daf-2* and *acds-10* are significant. All values are normalized to control integrated over the age range (ratios of areas under the curve; AUC).

longitudinal multiomics data being generated for UM-HET3 mice[81]. In ongoing mapping, this locus also modulates interactions of rapamycin with longevity using the same cases reported by the ITP in 2009[33] with an interaction effect with rapamycin of LOD 4.5.

We end the results section with a combined genetic and experimental analysis of *Vita9b*. This locus was mapped 23 years ago in an independent UM-HET3 cohort (Fig. 6a, Ref.[82] their *D9Mit10* locus) and this locus has also been validated in the BXD family of mice (data from Refs[83,84]). The replicability motivated us to perform a more intense dissection of its genetic effects. *D* and *H* haplotypes reverse polarity in males between T_{500} and T_{700} with two strong inflection points in late survivorships at T_{845} and T_{1050} (Fig. 6b, Extended Data Fig. 2o2). The *C* and *B* haplotypes have more uniform effects that peak at T_{785} (Fig. 6c). In females, effects are much more modest and are delayed until T_{800} (Extended Data Fig. 2o2). As in the case of *Vita1a*, these findings are also tight constraints on models and add useful priors for candidate gene selection once telomere-to-telomere (T2T) assemblies are available for all four progenitor haplotypes.

Vita9b spans 127 protein-coding genes for which missense variants are predicted to have moderate or high impact. The region corresponds to human Chr 3p21.1 (46 to 53 Mb) and 3q22.2 (130 to 138 Mb)[85]. We tested 15 *C. elegans* orthologs using RNAi knockdown (Fig. 6e)—a validated lifespan predictor[86,87]. Four knockdowns significantly altered activity after 14 days (Fig. 6f). Suppression of acds-10, an ortholog of murine *Acad11*, boosted motility from 18 to 27 days—approaching the *daf-2* control effect (Fig. 6f-h)[88]. In mice, *Acad11* is trans-activated by p53, enhances fatty acid β-oxidation, and increases expression with age across tissues[89–91]. Three other knockdowns reduced activity after 10 days (Fig. 6f-h): orthologs of *ACP3* (*pho-1*)[92,93], *PCBP4* (*pes-4*)[89–91], and *APEH* (*dpf-5*)[94]. All of these candidates align well with *Vita9b's* late-onset action, but none have yet been linked to longevity[72]. Three caveats apply: candidate gene analysis is biased by the depth of the literature, and sparsely studied genes risk being deprecated—the so-called ignorome[95]; second, *Vita9b* is likely to contain multiple linked variants that contribute to late onset disease[96,97]; third, candidate gene analysis without full T2T genome assemblies that include both short and very long polymorphisms is inadvisable.

Discussion

At least 59 loci shape mortality risks and lifespans of UM-HET3 mice with strong dependence on age. Some act early, others late, and many differ greatly by sex. A subset of loci have persistent genetics effects on mortality from T_{215} to very old survivorships and may modulate rates of aging. Males have many more early-acting *Vita* and *Soma* loci than do females, but this imbalance disappears with age. Doubling our previous sample size revealed new complex patterns of interactions while confirming six of seven loci we had detected[98]. Traditional genetics of aging has invariably defaulted to a single metric: the duration of lifespan. In contrast, our method tracks mortality across nested survivorships from puberty to old age. This simple actuarial innovation exposes the dynamics of mortality as a function of genotype, age range, and sex. Knowing when genetic effects appear and disappear provides an important context for molecular and cellular studies of age-dependent mortality risks across lifespans[10,99–101].

The UM-HET3 mice are a single genetic sibship derived from a cross of isogenic F1 hybrids, and like humans they segregate for millions of sequence variants. Unlike humans, UM-HET3 mice have a uniformly high minor allele frequency of 0.25—a benefit in terms of mapping power that contributed to our success in detecting loci even in the oldest 20% (N = 1568)—equivalent to studying the genetics of longevity in humans who have all reached their 90s[102,103]. We are able to control diet and environment and minimize many types of confounds—in particular, infectious diseases. There are two disadvantage of the UM-HET3 family: 1. loci cannot yet be mapped with high precision, although two *Vita* loci were hedged into 4–8 Mb intervals; 2. all haplotypes are heterozygous and it is therefore not possible to compute additive effect sizes or dominance deviations at *Vita* and *Soma* loci.

The age-dependence genetic effects. We listed four questions in the introduction. The first relates to age-dependence of lifespan loci. Some such as *Vita1c* and *Vita18a* operate only early in life with diminishing effects as early as 500 days. This type is much more common in males than females and these loci are likely linked to male-male competition, hormone status, and stress resilience[68,104]. Other loci act almost exclusively from 500 to 700 days (*Vita4a*, *Vita11a*, *Vita12a*). A final set affect only senescent mice (*Vita5a*, *Vita9b*, *Vita9c*). Our answer is that lifespan loci have very strong age-dependence, as do their interactions. The actuarial approach combined with correlated trait locus mapping[105] led to a collective 8.4x gain in numbers of *Vita* and *Soma* loci, all of which are securely placed into age-dependent classes that fortify theories of aging.

On genetics of lifespan and evolutionary theories of aging. Our second question was whether different types of age-dependent lifespan loci support evolutionary explanations of aging[40,43,44,106]. The first theory is that aging is caused by late acting variants that escape selection in natural populations due to high extrinsic causes of mortality—Haldane and Medawar's *mutation accumulation theory*[40,107]. This idea predicts a range of post-reproductive genetic effects, both good and bad with respect to longevity, that do not have detectible effects

on mortality early in life. In mice their impact should emerge only after about 500 days; either gradually as that of *Vita5a* in males or abruptly as that of *Vita1a* in females. The second theory is that aging is a consequence of fitness optimization and a careful compromise between reproductive investment and the necessity of self-maintenance and repair as a minimum up to the moment of reproduction[43,44,108]. This is Kirkwood's *disposable soma* theory[43]. The *Soma* loci collectively support this theory— they fit the model of loci that mediate a bio-energetic compromise between size and reproduction common in prey species adapted to volatile environments (*r*-type selection)[109,110]. The third theory is that aging represents a Faustian bargain between DNA variants that boost fitness early in life, but call for payment late in life—Williams' *antagonistic pleiotropy*[2,106,111]. Antagonistic pleiotropy is vivid in loci such as *Vita2a*, *Vita2b*, *Vita2c*, *Vita9b* (Fig. 6b) with effect polarities that invert with age. A simple prediction is that alleles that improve fitness before 400–600 days will be linked to higher reproductive success but increased late-life mortality—a pattern that is much stronger in males than females. The summary answer is that the dynamics of *Vita* and *Soma* loci provide a firm empirical bridge between theories and organismal processes of aging[2,100,112–114].

On sex and genetics of aging. Our third question addressed sex differences in lifespan. In previous work[98] we detected one female-specific locus on Chr 3 using the full survivorship and found no significant male-specific loci or gene-by-sex interaction effects, a limitation we attributed to low statistical power. We now define 13 loci with their strongest effects in males, 4 with their strongest effects in females, and 12 loci with their strongest effects when data are combined (Table 1). This male bias is even more pronounced among *Soma* loci—16 in males, 5 in females, and 9 combined. Sex differences in lifespan genetics are only well resolved by deep genetic dissection, mirroring previous findings in *Drosophila melanogaster*[5,115]. Sex differences can be so divergent that we are almost compelled to use the labels sexual *antagonism* or *reciprocity*, and this is especially true of epistatic interactions. Of course, this imprint of sexual competition in much stronger during the reproductive crescendo of life, contributing to trade-offs between body mass and life expectancy that are embedded in male *Soma* loci. After reproduction, male and female life expectancies converge. Natural selection has already had its say.

The integration of *Soma*, *Mass*, and *Vita* loci. Our final question focused on the trade-off between body size and lifespan. We have successfully converted "mere" correlations of weight-to-lifespan early and late in life into discrete *Soma* loci with strong sex- and age-dependent effects. *Soma* and *Vita* loci largely modulate expectancies autonomously, and while 12 *Soma* loci overlap *Mass* loci, their sex effects and dynamics rarely align (Fig. 5, Extended Data Fig. 4). The *Soma* loci directly exemplify antagonistic pleiotropy—defined here as modulators of the body mass-mortality trade-off—and these are the first such loci mapped in vertebrates with clarity. These loci recapitulate the equally explicit trade-offs in *Drosophila*[113–115]. Why the marked sex difference in genetic architecture of *Soma* loci? We propose the same explanation as for the *Vita* loci:

differential selection pressures favor fast growth and physical robustness or slow growth with better survival odd under resource limitations[55,116]. The independence of most *Soma* loci from *Vita* loci and from the *Mass* loci demonstrates that distinct biological processes orchestrate the set of mass-mortality equations in males and females.

Candidate gene analysis and the benefits of delayed gratification. Variation in *Vita* and *Soma* loci dynamics likely stems from allelic differences affecting growth rates, fitness, fecundity, and functional and genomic resilience across ages, and inevitably, their effects on disease timing. Wild mice die mainly of predation, disease, and cold stress[116,117] while laboratory mice die mainly of cancers and less commonly from renal, cardiovascular, and inflammatory disease[83,118,119]. Given the many intrinsic and extrinsic factors in play and the large size of most loci, we expect loci to often blend effects of several polymorphisms—the major challenge of complex trait analysis and systems genetics[9,120–122]. The second challenge of candidate gene analysis is when to say 'no, not yet'. In the results section we have balanced the promise against the risks of premature analysis and severe ascertainment bias. While oligogenic *Vita17a* and *VitaXa* loci are out of scope in terms of "cloning" gene *X* or SNP *Y*, *Vita1a* and *Vita9b* merit intense attention. In our opinion, several candidates—*ATP6VH1*, *ACAD11*, *ACP3*, *PCBP4*, and *APEH*—already warrant *in vitro* and *in vivo* tests and analyses of phenotypes and pathologies of males or females with defined genotype classes at specific ages. Resolving specific DNA variants that contribute to differences in mortality rates and lifespan ultimately relies on massive community resources and methodologies shared across organisms.

The dynamics of heritable variation in life expectancy in mice and humans. Genetic factors account for roughly 25% of variance in life expectancy of young adult humans[7,123], but heritability appears to increase as a function of age[31]. This trend has motivated searches for DNA variants in the oldest old humans[18,21,124]. In UM-HET3 mice we also find clear evidence of increasing heritability with age in males but less so in females (Fig. 2g,h). Surprisingly, in the oldest-old mice there is a decline in environmental variance, perhaps associated with the loss of lifelong companions. Does it make sense to focus on gene variants acting principally or exclusively in the oldest-old? We do not think so. They may well be happenstances of the shadow of selection. Far more important are those loci that modulate mortality from early stages of reproductive life through to senescence—the rate of aging modulators (Table 1). We highlighted 14 *Vita* loci of this type that may harbor variants that are both selectable and controllable.

Prospects. *Vita* and *Soma* loci can obviously be used to predict lifespan of, at a minimum, UM-HET3 mice, but we have not done so because maps and models need refinement. Higher density genotyping of the additional 19,000 UM-HET3 mice—including those treated with supplements that prolong lifespan—will provide a more secure foundation for prediction. Models will also need to be have parameters fine-tuned for environment, diet, sex, birth month, litter size, parity, and higher order terms such as social genetic effects among co-

housed mice[49,125]. ITP teams have spent 20 years rigorously testing 91 compounds for their lifespan-extending potential. More than 14 have succeeded—a 15% hit rate[32–34,126–134], but with a strong bias in favor of positive effects in males (updated through to 2021 cohort, R.M. personal communication). Rapamycin is one welcome exception with strong beneficial prolongevity effects in both sexes—but this drug like all others will be strongly modulated by many gene-by-drug interactions. One person's poison is another's cure. Those agents that have nominally "failed" have not truly failed until they have also been tested for gene-by-drug interactions. We have shown here that all ITP drugs can now be placed within a known constellation of loci that modulate mortality, potentially guiding interventions to extend human health and longevity[135,136].

Materials & Methods

The UM-HET3 sibship

UM-HET3 mice are progeny of a cross between two types of F1 hybrids—female F1s from matings of BALB/cByJ (C) dams to C57BL/6J (B) sires, and male F1s from matings of C3H/HeJ (H) dams and DBA/2J (D) sires. These four inbred progenitors are abbreviated CBy, B6, C3H, and D2 when referring mice and strains, and abbreviated *C*, *B*, *H*, and *D* in italic when referring to genotypes and haplotypes. They were selected to maximize phenotypic diversity. Young virgin F1 males and females were distributed from the JAX production facility at The Jackson Laboratory (TJL) to ITP research colonies at TJL in Bar Harbor Maine (JL), the University of Michigan in Ann Arbor Michigan (UM), and the University of Texas Health Science Center in San Antonio (UT). Breeding cages were set up each spring. First litters were not used. All subsequent litters were used at UT, litters with 6 or more pups were used at JL, and those with 7 of more were used at UM. Weanlings were entered into the study over the next seven months. Mice lived together from weaning at 19 to 21 days and without replacements until their deaths[137]. As a result, most mice live solo after 1000 days, a factor to consider with respect to mortality risks but not yet integrated into the analysis here.

All mice in the first four cohort years were born between April 2004 and Jan 2008. For these years we have numerically well-balanced DNA samples from all sites. Almost no animals were generated in 2008 due to a funding gap. All mice in the final cohort years used in this study were born between July 2009 and March 2013. The 2009 cohort includes mice from all sites, but 2010 and 2011 include mice only from UM and UT. Cohort years 2012 and 2013 include mice only from UM. -HET3 mouse in this studied died on Dec. 21, 2015. Only a very small percentage of mice (<10%) were born January through April. Mice were weighed at 42 ± 2 days, and at 183 days (6 months), 365 days (12 m), 584 days (18 m), and at 730 days (24 m) with a timing error of approximately 7 days. The last UM-HET3 mouse in this study died on Dec. 21, 2015. In all years, only a very small percentage of mice (<10%) were born from January through April. Mice were weighed at 42 ± 2 days, and at 183 days (6 months), 365 days (12 m), 584 days (18 m), and at 730 days (24 m) with a timing error of approximately 7 days.

The UM-HET3 sibship segregates for ~10.6 million sequence variants (Supplementary Table 1 zip-file). All UM-HET3 mice inherit *C* and *B* haplotypes from their F1 mothers and *H* and *D* haplotypes from their fathers. As a result, sibs segregated for four genotypes (four two-way combinations of maternal and paternal haplotypes) on all autosomes—*CH*, *CD*, *BH*, and *BD.* Females inherit one entire non-recombinant *H*-type Chr X from their paternal grandmothers and a potentially recombined Chr X from their mothers (recombinations between *C* and *B* haplotypes only, see Fig. 3g). As a result, females have either *CH* or *BH* genotypes. Hemizygous males inherit a potentially recombined *C* or *B* Chr X from their mothers. All mitochondria are derived from maternal grandmothers (*C*) and Chr Y is derived from paternal grandfathers (*D*).

We genotyped 6,872 UM-HET3 mice for which we had full lifespan estimates (*N* = 3252 females, *N* = 3620 males). Of these genetic siblings 6,438 passed all genotype QC steps at 893 high-quality markers (*N* = 3401 females, *N* = 3037 males; see *Genotyping and Marker QC*). To ensure balanced numbers by sex later in life, every ITP cohort initially consists of 51 male and 44 female weanlings per year, per site, and treatment category, but with two-fold more common untreated controls at each site. This was done to enable overly aggressive males and any wounded animals to be removed while balancing male and female numbers later in life—almost always before 550 days. The earliest minimum inclusion age in this study is T_{42}, the pubescent age at which tails were docked for tissue acquisition, an age equivalent to about 12 years in humans[138]. For numerical convenience we set the first truncation age at T_{35}. To compensate for two-fold higher male mortality in the first two years of life (33% vs 16%) we included 12% more males than females in the T_{42} survivorship. The earliest death was at 46 days. This left us with a small surplus of 227 males at T_{365}, but by T_{560} numerical balance was restored and there were 2930 females and 2929 males. This age corresponds to roughly 56 years of age in humans (Ref.[139] their fig. 20.3). All individual-level data, metadata, and survivorships, and mortalities per 15-day interval are provided in Supplementary Table 2.

We genotyped two major categories of mice—those not treated with any dietary intervention and mice treated with a dietary supplement that did not modify lifespan significantly on a per-drug basis using standard statistical criteria[126,130,140]. These latter mice have been referred to as *No Drug Effect* (NDE) cases. However, when data are combined across the entire class of these individually "ineffective" agents from 2004 to 2013, there is in fact a highly significant multi-supplement that is positive on lifespan (Results). A better term going forward is *No Significant Effect* (NSE).

Husbandry

Mice were weaned into same-sex cages—three males or four females per cage—at 20 ± 1days[32]. From 2004 until 2013, all sites used NIH-31 standard diets. For breeding cages, UM used Purina 5008, UT used Teklad 7912, and JAX used Purina 5K52. For mice up to ~122 days, UM used Purina 5001, UT used Teklad 7912, and JAX used Purina 5LG6. After 2004, the control diet LabDiet 5LG6 was used by all sites. Mice were monitored daily for signs of ill health and aggression. Mice were euthanized if moribund. Tails were obtained at 42 ± 2 days for DNA extraction. Body weight at this age was acquired for 2459 mice, and at half-year intervals for 4688 mice at 183 days (6 months), down to 2208 mice at 730 days (24 m). Our analysis includes four experimental variables—sex, site, dietary drug treatment, and cohort year (Supplementary Table 3). Treatments are listed on *Mouse Phenome Database ITP Portal* under the acronyms 4OHPBN, CAPEhi, CAPElo, Cur, Enal, FOhi, FOlo, GTE, HBX, I767d, MB, MCTO, MET, NFP, OAA, Res07, Reshi3, Reslo3, Simhi, Simlo, and UA.

DNA extraction from tails, sequencing and sequence alignment

Tail tissue was processed using the MagMAX magnetic-bead extraction system (Thermo Fisher Scientific) and genomic DNA was quantified using a Qubit 4 fluorometer and a high-sensitivity DNA assay kit (Thermo Fischer Scientific). Locus-specific PCR primers were designed using *BatchPrimer3*[141] to generate 180 bp amplicons. They were mixed using an optimized Hi-Plex approach at Floodlight Genomics LLC (Knoxville, TN). Sample-specific 12 bp barcodes were added and amplicons were pooled[142]. Primer sequences for SNP markers with rs-type identifiers are provided in Supplementary Table 4). The amplicons were sequenced to an average of 1000X per targeted locus on an Illumina NovaSEQ (2x150 bp) at Admera Health LLC (Plainfield, NJ). Data were demultiplexed and FASTQ files used for genotyping. FASTQ files were aligned to *Mus musculus* GRCm38.p6/mm10 reference using *Bowtie 2* (version 2.3.4.1)[143]. BAM files were sorted and indexed using *samtools* (version 1.6)[144], and read group information was added using *picard* tools (version 2.14.1).

Variant calling

We called short sequence variants using *bcftools*[144] in three steps: 1. we created text pileup output for all BAM with *mpileup* at a mapping quality of 30; 2. we called using default settings; 3. we removed variants with a read depth <100 across all samples and a QUAL score <100. Sequencing depth per case was used as an additional criterion for filtering. Sequence for C57BL/6J, C3H/He, and DBA/2J was downloaded from the Wellcome Sanger Mouse Genome Project[145] (www.sange.ac.uk/data/mouse-genomes-project) and that for BALB/cByJ was generated by Beierle and colleagues[146]. From these files we extracted variants that differ among founders (Supplementary Table 1, a large *zip* file). Variants were called in three steps as above, the differences being that the minimum depth was reduced to 10x and QUAL score to ≥30. Variants that were called reliably in all founders were advanced for genotype phasing and mapping. VCF files with variant data on UM-HET3 and their founders are provided in Supplementary Table 5.

Genotyping by Sequenom MassARRAY

Tails were plated in deep-well plates and sent in three different batches to Neogen Corporation (Lincoln NE). Individuals were genotyped by SNP genotyping by Sequenom MassARRAY MALDI-TOF mass spectrometry[147] at a maximum of 270 markers. Fifty markers were removed after QC, based on deviations from expected allele frequency (0.35 < frequency < 0.65). We chose pairs of linked markers to define maternal and paternal chromosome genotypes.

Phasing SNP genotypes

SNP genotypes were phased using R v4.0.2 (*R Development Core Team* 2005; script at *github.com/DannyArends/UM-HET3*). We generated fully phased haplotypes for all sets of maternal and paternal autosomes and Chr X. Markers fall into those that unambiguously define maternal haplotypes (N = 486)—*C* vs *B* alleles (denoted by lines in pink Fig. 1c); those that define paternal haplotypes (N = 396)—*H* vs *D* alleles (blue lines

in Fig. 1c). We generated diploid genotype probabilities at all positions from phased chromosomes using the *calc.genoprob()* function in R/qtl. Markers were reviewed and those than had a call rate <30% were excluded. When we plot genotype and/or haplotype effects (Extended Data Figs 1 and 2), we call genotypes and haplotypes when imputation certainty is greater than 80%. We used R/qtl to estimate number of recombinations per mouse. The mean recombination number was 25.1 ± 8.6 SD. Just over 370 animals had recombination numbers more than two standard deviations above this mean. We excluded 59 mice that had more than 80 recombinations—likely to be caused by sample cross-contamination. The final genotype files are available at *GeneNetwork.org*[148–150] by setting *Species* = Mouse, *Group* = Aging Mouse Lifespan Studies (NIA UM-HET3), and *Type* = DNA Markers and SNPs and pressing the *Info* button. Supplementary File 6a lists all genotypes, and Fig. 6b is the R/qtl cross object used for most analysis.

Genotype quality control

Markers and individuals with greater than 90% missing data were removed from further analysis (*N* = 333). We converted data from genotypes into parental haplotypes (see section: *Phasing SNP Genotype*s). Markers were checked for Mendelian inheritance errors and removed when missing the data rate after conversion exceeded 90%. We integrated MonsterPlex and Sequenom marker sets based on genomic positions. We inspected the marker map for linkage between neighboring markers, and removed a single marker (Chr 4_58784823) which did not show linkage to its neighbors. We also removed 20 individuals that died of unnatural causes and 22 that we inadvertently genotyped that had received an effective drug supplement. Finally, we constructed an R/qtl cross-object for imputation using the remaining mice, imputed their haplotypes based on the full population (*N* = 6,438) (Supplementary Table 7).

Inversions in the UM-HET3

There is a large inversion on Chr 6 of the C3H/HeJ progenitor strain[151] between 51 and 94 Mb and may affect map precision (Table 1, 2). The recombination fraction in this interval is 0.00025 versus an expectation of 0.21. At least 42 Mb of the paternal chromosome is locked in linkage. We detected a total of 13 potential inversions ranging in size of 3.5 to 54 Mb. Six suppress recombination on the maternal chromosome and 7 suppress recombination on the paternal chromosome (Supplementary Table 8). There is overlap of maternal and paternal inversions on Chrs 4, 7, and 11.

Lifespan estimates depend on age of entry into a cohort

Based on work by König and colleagues[55,116] we know that in wild commensal populations of mice, 35–40% of pups do not survive beyond weaning. At birth, mean lifespan can be as low as 196 days. By 13 days, the mean expectancy has improved to 250 days for males and 500 days for females. We make these points to emphasize that lifespan estimates are made with reference to an operational starting point—a minimum ascertainment base age for a population. Researchers often incorrectly imply that mean lifespan is estimated from

the date of birth, but this neglects earlier and often unknown numbers of deaths. In our case we can only measure lifespan for UM-HET3 progeny that lived to be pubescent juveniles. When we say that the mean lifespan of the 6438 sibs in this study is 844 ± 210 SD days (median of 870 d), we mean that this is the mean age at death conditioned on a mouse having lived to at least 42 ± 2 days—the age at which tail tips were taken for DNA extraction.

In a similar way we can determine the mean lifespan or life expectancy of the survivorship subsets of UM-HET3 mice that lived to be at least 185, 365, 545, 725, or 1100 days (roughly 0.5, 1, 1.5, 2, and 3 years, respectively). The mean conditional lifespans of those five survivorships or age cohorts are 847 ± 206 SD days, 861 ± 188, 890 ± 160, 941 ± 126, and 1162 ± 54 SD days. The oldest mouse was a female that died at 1456 days. We refer to these different ages at which lifespan can be computed as either survivorships or cohorts.

The actuarial procedure consists of sequentially studying progressive older and smaller survivorships from the radix population of 6438 mice in Fig. 1a. The minimum inclusion age is 42 days. Between T_{42} and T_{50} days a single male died. We truncated the survivorships upward from T_{50} to T_{1100}, in 15-day steps. Although all individuals have accurately known lifespans, we sometimes use the term *life expectancy* to emphasize that our approach exploits lifespan data in an actuarial context conditioned on have reached a specified age. We speak of the life expectancy of mice that have reached 1100 days in the same way that we would speak of the life expectancy, not the lifespan, of 70-year-old humans.

The actuarial mapping strategy is affected both by lower sample size and by right skew at higher truncations. To ensure that our results are not affected by this, we used three approaches. First, we use a non-parametric quantile regression in combination with standard parametric mapping to make sure associations are detected using both methods[152]. Second, we limited ourselves to a maximum truncation age of T_{1100}. Third, we used a time-dependent hazard function to validate *Vita* loci.

We tested a complementary approach for mapping under the assumption that loci contribute to variation in the time-dependent hazard function as in our previous[98] but with refinements. We carried out a test at each marker of the null hypothesis that the (time-dependent) hazard function of death does not depend on genotypes. To do this, we used a model where the hazard function is allowed to depend smoothly on age with haplotype and baseline covariates, using natural splines with three degrees of freedom. For computational tractability we created risk sets with 50-day window[153].

Implementation of actuarial mapping

We mapped in 15-day survivorship steps from T_{42} to T_{1100}. Mapping was performed using both conventional four-way mapping of genotypes at 893 makers (Fig. 1c) or by restricting analysis each of the parental haplotypes—*C* versus *B* on the maternal chromosomes (N = 497 markers), and *H* versus *D* on the paternal chromosomes (N = 396 markers). Note that Chr X only segregates for maternal *C* and *B* haplotypes in both sexes (Fig.

3f,g). In general, mapping all four genotypes provides better power. This method defined all loci in Table 1 and full LOD scores across all survivorships are illustrated in Extended Data Figs. 1, 2. The null model (model(H_0)) and alternative model (model(H_{alt})) were fitted at each marker using the following linear models:

$$\text{model}(H_0)\text{: lifespan} = \text{sex} + \text{site} + \text{cohort} + \text{treatment} + \text{error}$$

$$\text{model}(H_{alt})\text{: lifespan} = \text{sex} + \text{site} + \text{cohort} + \text{treatment} + \text{gtp} + \text{error}$$

Sex has two levels (M, F), *site* has three levels (JL, UT, UM), *cohort* year has nine levels (no animals were generated in 2008), *treatment* has two levels—untreated controls and cases that received a drug that had no significant effect on lifespan. The gtp (***g***eno***t***ype ***p***robability) term is a *N* row by four-column matrix, where *N* is the number of individuals used in the mapping, and columns are genotype probabilities for markers computed by R/qtl (v 1.48-1)[154,155]. Sex was dropped as a co-factor from the regression model when mapping was stratified by sex. LOD scores were computed by comparing the fit of the null model with the fit of the alternative:

$$\text{LOD} = (n/2) * \log_{10}(\text{sum}(\text{residuals}(H_0)^2) \,/\, \text{sum}(\text{residuals}(H_{alt})^2))$$

Mapping on Chr X requires special care due to the four-way cross structure and greater difficulty defining highly reliable markers for haplotype, particularly close to both telomers.

Effect size plots resolve survivorship differences by genotype and sex

We use the four-way mapping algorithm implement in R/qtl[155,156] while controlling for sex, site, cohort year, and drug treatment. We compute maps for survivorships starting from T_{42} up to T_{1100} (Fig. 1a,d,e,f). We introduce a new type of actuarial plots in Fig. 1b,d,e. The x-axis defines the minimum inclusion age (T-age) of each survivorship. The expected increase in error terms in older survivorship with lower sample sizes are mitigated by the reduced range over which animals die within progressively older survivorships—from 1410 days at T_{42} to 356 days at T_{1100}. Errors of lifespans of survivorships are relative stable—from 844 days ± 210 SD in the T_{42} base population (SD/ range of 15%) to 1162 ± 54.4 SD in the last T_{1100} survivorship (SD/range of 15%). When interpreting effect size plots note that increases and decreases in mortality rates among subgroups are relative to the mean lifespan of that T-age.

In the present paper we focus only on upward truncation, but we have also tested retrograde truncations that exclude older survivorships—that work by truncating downward. For example, T_{730} is the designation for the exitship of all animals that died before day 731—the converse of the T_{731} survivorship that includes all animals that lived to at least 731 days. We also selectively use two-sided or dual truncations to isolate mortality age ranges—for example the exitship of males that died between 365 and 730 days designated the $T_{365\text{-}730}T$ exitship (Supplementary File 14).

Significance testing for actuarial time-series analysis

We evaluated the significance of mapping results across two axes: 1. the spatial location of markers and their independence across the genome; and 2. the temporal axis and the number of effectively independent actuarial tests. We mapped using 893 markers but given the significant linkage between markers we effectively tested about 442 independent genome locations. This number of independent tests was estimated using the *simpleM* method with a block length ranging from 10 to 500 markers and a 10-marker step size[157]. The threshold at a genome-wide type 1 Bonferroni error rate of 10% is 3.65 LOD ($-\log_{10}(0.1 / 442)$, at 5% it is 3.95, and at 1% is 4.65. These are conversative thresholds. For maternal and paternal maps, the density of recombination is reduced by half, and corresponding thresholds are 3.44, 3.65, and 4.34.

Positional confidence interval using the typical 1.5 LOD-drop in linkage[45]. We also estimated temporal range of action of loci, defined as the T-ages over which a locus has strong effects. The start and stop T-ages are those that immediately precede or succeed survivorships that are genome-wide significant. For example, if linkage is above LOD of 3.95 from T_{365} to T_{725}, then the T-age CI of the locus from T_{350} to T_{740}. This criterion is not conservative when only a few survivorships have significance. In this latter case, we define the T-age range that brackets the peak T-age by a >1.5 LOD drop.

Finally, we evaluated the impact on significance testing of mapping multiple nested survivorships. We evaluated this risk using a Cauchy combination test[158] at each marker across all survivorships (Table 1). Cauchy *P* values were adjusted for multiple testing using a Benjamini and Hochberg correction to account for multiple testing across markers, and the Cauchy $-\log P$ in Table 1 of ≥1.50 is significant at a *P* of less than 5%.

Locus assignment and candidate gene region determination

Locus names are prefixed *Vita*, *Soma*, and *Mass* type identifiers followed by the chromosome location and a letter suffix (*Vita1a*, *Soma2b*, *Mass11c*). When the 95% confidence intervals of two adjacent QTLs overlap, and the genotype effects are the same, loci are generally assigned the same *Vita* identifier. For such "merged loci", the 95% CI is reduced to the overlapping interval. Determining whether a locus is detected in different subsets of the cohort is somewhat subjective, examples being *Vita3a* and *Vita14b* that could have been split into two loci (e.g., *Vita3a1* and *Vita3a2*) by sex and T-age. We provide data for linkage scores in all three categories (sexes combined, females, and males) for *Vita* loci (Supplementary Table 9), *Soma* loci (Supplementary Table 10), and *Mass* loci in (Supplementary Table 11).

Testing for sex interactions at *Vita* loci

There are significant differences between male and female stratified survivorship maps. To investigate this formally and to detect significant sex-marker interactions modulating age-specific lifespan we tested sex-interactions of *Vita* loci at the T-age with the peak LOD (Fig. 3a). We computed the LOD score difference of two models against each other:

```
model(H0): longevity = sex + site + cohort year + treatment + gtp + error
model(Halt): longevity = sex + site + cohort year + treatment + gtp + gtp:sex + error
```

Since we are only interested in significant sex-interactions at previously detected *Vita* loci but excluding *VitaXa*. We used a stringent Bonferroni correction based on 28 markers. A LOD scores above 2.75 is significant ($-\log_{10}(0.05/28)$).

Testing pair-wise epistatic interactions between *Vita* loci

A two-dimensional analysis of marker-marker interactions affecting life expectancies was performed by testing the following models against each other in four survivorships—T_{42}, T_{365}, T_{740} and T_{905}.

```
model(H0): lifespan = sex + site + cohort year + treatment + gtpm1 + gtpm2 + error
model(Halt): lifespan = sex + site + cohort year + treatment + gtpm1 + gtpm2 + gtpm1:gtpm2 +
error
```

We computed the difference in fit. To limit numbers of tests, we again only test interactions between 28 autosomal *Vita* loci (Table 1) but excluded any pair of loci located on the same chromosome (Fig. 4a). This results in the matrix of 359 non-syntenic tests per sex. We used Bonferroni adjustment for multiple testing leading to a threshold of $-\log_{10}(0.05/359) = 3.85$. We mapped epistatic interactions at four representative survivorships: T_{42}, T_{365}, T_{740}, and T_{905} (Fig. 4 and Supplementary Table 12).

Mapping *Soma* loci that modulate correlations between body weight and life expectancy

Body weights were measures at 42 days (right before tails were biopsied for genotyping); and at 183, 365, 548, and 731 days (6, 12, 18, and 24 months). We used these data to map loci for body weights for both sexes so that we could align and compare body weight loci with *Vita* and *Soma* loci (e.g., Fig. 5a-c). Sample sizes for mapping *Mass* loci range from a low of 2459 at 42 days to a high of 4688 at 183 days (Supplementary Table 13). Models used are like those used for mapping *Vita* loci, but the variable is body weight at each of five ages.

Actuarial analysis of the correlation between body weight to life expectancy by sex

To investigate the effects of body weight on lifespan, we adjust body weight and lifespan using the model:

```
Lifespan(adjusted) = mean(Lifespan) + residuals(Lifespan ~ Sex + Site + Cohort + Treatment)
BW(adjusted) = mean(BW) + residuals(BW ~ Sex + Site + Cohort + Treatment)
```

This model includes mice for which we have lifespan and weight data at one or more of the five weight ages. We computed the sex-stratified Spearman rank-order correlations between weights at 42, 183, 365, 548, and 730 days with lifespan in 15-day increments (Fig. 5d-p). We compute the $-\log P$ of the difference in correlation between males and females using the *cor.test* function in R. The average correlation in the combined population between adjusted body weight at 183 d (~6 months) and adjusted lifespan is rho = –0.206. When computed for males, correlation is stronger (rho = –0.284), while it is weaker for females (rho = –0.110).

***Soma* Correlated Trait Locus (CTL) mapping**

We used CTL mapping[105] to determine if a distinct set of loci modulate correlations between body weight and subsequent lifespan compared to either *Vita* or *Mass* loci. Before using this procedure, we adjusted body weight and lifespan using sex, site, cohort year, and drug treatment as covariates. At each marker we stratified survivorships based on genotypes. Ideally, the sample size for each subgroup would be above 400, but in some cases, N was as low as 200 due to genotype uncertainty and to the lower sample sizes at T_{42} ($N = 2549$) and T_{730} ($N = 2208$). We computed robust Spearman's rank correlations for each genotype with $N > 100$ and the z-scores associated with differences:

```
z = 0.5*log((1.0 + cor)/(1.0 – cor))
```

Here `cor` is a four-value vector containing the observed correlations for *CH*, *BH*, *CD*, and *BD* genotypes. We compute the sum of squares (`sumOfSq`) by multiplying the observed sample sizes (`ss`) of the *CH*, *BH*, *CD*, *BD* genotypes to the squared z-scores:

```
sumOfSq = sum(ss * z²)
```

We compute the squares of sums (`sqOfSum`):

```
sqOfSum = sum(ss * z)²
```

Using these values, and the sum of the sample sizes on which each correlation is based, we compute the critical value (`Cv`) which follows a chi-square distribution under the null hypothesis that all correlations (z- scores) are from the same distribution:

```
Cv = sumOfSq – (sqOfSum / sum(ss))
```

The `Cv` is converted to a P value using the chi-squared distribution using the *pchisq()* function in R, with P[X > x] and three degrees of freedom (number of genotypes – 1).

We adjust the significance threshold for multiple tests using the *p.adjust* function in R at a 5% FDR[159,160]. The 5% FDR threshold is approximately 2.75 –log$P$. While still stringent, this threshold is less harsh than that applied to *Vita* loci that use a highly conservative Bonferroni correction. Our rationale for this difference is our use of conversative non-parametric rho for comparing correlations of weight to lifespan. Differences in correlation correspond to days gained or lost relative to an average individual that can be converted to effect sizes measured in days gained or lost per gram of weight. We computed the linear regression coefficient for weight on lifespan for the four genotypes as:

$$\texttt{Lifespan}_{\texttt{(adjusted)}} = \texttt{mean(Lifespan)} + \beta \times \texttt{bodyweight}_{\texttt{(adjusted)}}$$

where `mean(Lifespan)` is the intercept of the total population (all genotypes combined), while the β coefficient is the estimated effect size of weight on lifespan based on the subpopulation defined by each genotype. This leads to effect sizes relative to an averaged mouse. There are caveats with respect to interpreting these effects because they are computed relative to this idealized mean, but values should give readers a sense of effects of *Soma* loci on life expectancies.

Broad-sense haplotype-based heritability of *Vita* loci

We compute broad-sense genotype-based heritability by fitting a full model including the haplotype probabilities of the 29 top markers of all *Vita* loci:

$$\text{lifespan}(_{T-age}) = \text{sex} + \text{site} + \text{cohort} + \text{treatment} + \text{gtp}_{Vita1a} + \text{gtp}_{Vita1b} + \ldots + \text{gtp}_{VitaXa} + \text{error}$$

Broad-sense haplotype-based heritability is estimated by fitting this model to all survivorships. When stratifying by sex, sex is dropped from the model as well as from the H^2_e component described in the computation of environmental variance component below. Computing heritability is done by taking the following approach, adapted from Falconer[161] and Lynch and Walsh[162] using five steps:

Step 1: The vector of partial total variances (PTV):

$$ptv = (\sigma^2 - \sigma^2_{residuals}) / r$$

Step 2: An adjustment factor—the sum of the mean sum of squares for the fixed effect including the residual variance:

$$adj = sum(\sigma^2) / r$$

Step 3: The contribution of each parameter in PTV to the model:

$$C^2_p = ptv / adj$$

Step 4: The total broad-sense genotype-based heritability:

$$H^2_h = C^2_{Vita1a} + C^2_{Vita1b} + \ldots + C^2_{VitaXa}$$

Step 5: The environmental variance:

$$H^2_e = C^2_{sex} + C^2_{site} + C^2_{cohort} + C^2_{treatment}$$

where σ^2 is the vector containing all the means of sums of squares (including the residual) computed by the ANOVA model. $\sigma^2_{residuals}$ is the residual mean sum of squares. *r* is the average number of replicates for each genotype. H^2_h can be interpreted as the broad-sense genotype-based heritability as a sum of all *Vita* loci. H^2_e is the environmental variance estimate of the known environmental covariates. Unexplained variance H^2_u can be computed as:

$$H^2_u = 1 - (H^2_h + H^2_e)$$

To obtain upper and lower bounds on H^2_h and H^2_e we generated 50 bootstrap resamples and fit the ANOVA model to each using a random subset of 90% of the survivorship. We computed median and standard deviations across all bootstraps to estimate errors of H^2_h and H^2_e as a function of survivorship T_{age}.

Candidate genes analysis

All annotated features located within the 95% CI were downloaded using *biomaRt*[163]. We applied a several criteria to prioritize positional candidate genes: (1) first, we considered only the protein coding genes that reside in the 95% confidence intervals; (2) we then selected genes with annotated non-synonymous SNPs segregating in the population, and these were further ranked by the potential deleterious effect based on the ENSEMBL *Variant Effect Predictor* (VEP)[164]; (3) another priority score for the candidate genes was based

whether they were listed as aging and longevity genes in GenAge[165]. We also compared our positional candidate genes against known human, *C. elegans*, *D. melanogaster*, and *S. cerevisiae* genes reportedly associated with age in GenAge. To accomplish this, we use *biomaRt* to convert mouse gene symbols into the corresponding species orthologues gene, to allow us to match genes across species.

Different gene sets from *Vita* loci were tested for over-representation with WebGestalt[166] for over-representation analysis based on gene ontologies and molecular pathways (KEGG, REACTOME). We performed this analysis using three categories of gene set and background sets: 1. All protein-coding genes in *Vita* regions (N = 6975) versus the whole genome. 2. All protein coding genes with medium and high impact variants (as determined by the VEP) in *Vita* regions (N = 2502) versus all protein coding genes in *Vita* regions. 3. All protein coding genes with high impact variants (as determined by the VEP) in *Vita* regions (N = 409) versus all protein coding genes in *Vita* regions. Given the high number of G protein-coupled receptors (GPCRs) and olfactory receptors (OLFR) in our *Vita* regions, we repeated these three analyses while excluding GPCRs and OLFR. This reduces the size of the different gene sets to all protein-coding genes (N = 6112), those with either medium or high impact variants (N = 2354), and those with only high impact variants (N = 382).

C. elegans candidate gene screening of *Vita9b* candidates

We searched for potential *C. elegans* orthologs by searching for the protein-coding genes within the *Vita9b* **locus using Ortholist2**[167]. From the list of potential orthologs, we screened C41D11.3 (ortholog of murine *Csrnp1*), F52F12.1 (*Slc22a13*), H09G03.2 (*Frmpd1*), C12C8.3 (*Trim71*), F30A10.3 (*Ip6k2*), T22C8.2 (*Hyal1*), L4440 (empty vector control) and daf-2 (positive control) from the Ahringer RNAi library[168]. The sequence-verified single RNAi clones listed above were inoculated in 10 mL LB with ampicillin (100 µg/ml) and tetracycline (50 µg/ml) overnight at 37 °C. The next day 5mL of LB with 0.5mM isopropyl b-D-1-thiogalactopyranoside was added and inoculants were incubated for 30 min at 37 °C with shaking for pre-induction. The bacterial inoculants were centrifuged (3700 rpm for 15 min) and the pellet was resuspended in 10mL liquid NGM with 50 µg/mL IPTG, 100 µg/mL ampicillin and 13.32 mg/ml nystatin.

Gravid adult stage TJ1060 [*spe-9(hc88)*;*rrf-3(b26)*] *C. elegans* were synchronized by bleaching. Resulting L1 stage worms were suspended in concentrated heat-inactivated OP50 bacteria in liquid NGM and transferred into U-bottom 96-well plates in a final volume of 100 µL. The worms were grown on an orbital shaker (Heidolph Titramax 1000) at 600 rpm until they reach L4 stage (approximately 2.0–2.5 days) at 25 °C to prevent progeny production. When worms reached L4 stage, 20 µL of bacterial inoculant of each RNAi clone were added into single wells of the U-bottom 96-well plates containing worms. At least 30 worms per well and 8 wells per clone were used for screening. The MicroTracker (InVivo Biosystems) system was used to measure motility in liquid in 96-well plates by infrared beam breaks. Plates were measured daily for a period of at least 90 min.

Exploratory data analysis, replication, and extension of UM-HET3 data by readers and students

All primary data used in this study (and more) is available at www.genenetwork.org (GN) along with tools for truncation, mapping, and basic analysis of correlations between variables such as lifespan and body weight. We provide a text step-by-step guide in Supplement File 14 (MS Word and RTF formats) on how to replicate findings described in this paper and how to extend the analysis using for example retrograde truncations and dual truncations. These functions are extremely useful for dissecting the both survivorships and exitships over different ranges of T-ages.

Author contributions

D.A., R.W.W., J.A., E.G.W, D.G.A., K.M.M, and R.A.M. were responsible for conceptualization. ITP colony management and informatics were directed by R.S., D.E.H., and R.A.M. Tissue and DNA sample processing and data curation was managed by S.R., D.G.A., V.D., K.L., A.C., L.L., D.A., R.A.M., and J.F.N. Statistical and bioinformatics was conducted by D.A., S.S., D.G.A., K.W.B, R.W.W, J.P.M., and M.R.M. Code development for mapping of UM-HET3 was developed by K.W.B., D.A., S.S., P.P., Z.S., and R.W.W. *C. elegan*s analysis by M.A.M, O.A.A., and S.J.M. Manuscript and illustrations by R.W.W., D.A., and E.G.W., with review and edits by all authors.

Acknowledgments

This work was supported by grants from the NIH R01AG043930 (R.W.W.), NIH R01AG070913 (R.W.W.), NIH R01AG075813 (D.G.A.), the University of Tennessee-Oak Ridge National Laboratory Governor's Chair in Computational Genomics for genotyping, and the University of Tennessee Center for Integrative and Translational Genomics for data processing (R.W.W., D.G.A, D.A., L.L. S.R. P.P, A.C.,Z.S.), NIH grants NIA U01AG025707 and U01AG022308 (D.E.H.), U01AG022303 and OAIC P30AG024824 (R.A.M), U01AG022307 and P30-AG13319 (R.S.), and U01AG025707 and R01GM123489 (P.P., S.S., K.W.B., R.W.W.), Ecole Polytechnique Fédérale de Lausanne (J.A.), European Research Council (AdG-787702) (J.A.), Swiss National Science Foundation (310030B160318) (J.A.), AgingX: Swiss Initiative for Systems Biology RTD 2013/153 (J.A.), NIH NIDA P30DA044223 (S.S., R.W.W.), NIH R21AG055841 and R56AG066625 (K.M.)

Competing interests

The authors declare no competing interests.

Additional information

All primary data and many analytic tools associated with this papers available at www.genenetwork.org. For example, this URL will take reader directly to ITP lifespan data for 23,876 mice, including all mice analyzed in the work.

https://genenetwork.org/search?species=mouse&group=HET3-ITP&type=Phenotypes&dataset=HET3-ITPPublish&search_terms_or=10000%0D%0A&search_terms_and=&accession_id=None&FormID=searchResult

Code used in mapping and analysis available at https://github.com/DannyArends/UM-HET3

Supplementary files are available upon request to: RW Williams (labwilliams@gmail.com) and D Arends (Danny.Arends@gmail.com). Files are large collectively too large to incorporate into this bioRxiv submission. Correspondence and requests for additional material can be addressed to RW Williams.

© The Authors

References

1. Maynard Smith, J. Review lectures on senescence - I. The causes of ageing. *Proc. R. Soc. Lond. B.* **157**, 115–127 (1962).
2. Rose, M. & Charlesworth, B. A test of evolutionary theories of senescence. *Nature* **287**, 141–142 (1980).
3. Gelman, R., Watson, A., Bronson, R. & Yunis, E. Murine chromosomal regions correlated with longevity. *Genetics* **118**, 693–704 (1988).
4. Schächter, F., Cohen, D. & Kirkwood, T. Prospects for the genetics of human longevity. *Hum Genet* **91**, 519–526 (1993).
5. Nuzhdin, S. V., Pasyukova, E. G., Dilda, C. L., Zeng, Z. B. & Mackay, T. F. Sex-specific quantitative trait loci affecting longevity in *Drosophila melanogaster*. *Proc Natl Acad Sci U S A* **94**, 9734–9739 (1997).
6. Vaupel, J. W. *et al.* Biodemographic trajectories of longevity. *Science* **280**, 855–860 (1998).
7. Mitchell, B. D. *et al.* Heritability of life span in the Old Order Amish. *American Journal of Medical Genetics* **102**, 346–352 (2001).
8. Mackay, T. F. C. The nature of quantitative genetic variation for *Drosophila* longevity. *Mechanisms of Ageing and Development* **123**, 95–104 (2002).
9. De Luca, M. *et al.* Dopa decarboxylase (*Ddc*) affects variation in *Drosophila* longevity. *Nat Genet* **34**, 429–433 (2003).
10. Miller, R. A. Genes against aging. *J Gerontol A Biol Sci Med Sci* **67**, 495–502 (2012).
11. Atzmon, G. *Longevity Genes: A Blueprint for Aging*. vol. 847 (Springer, New York, 2015).
12. Soerensen, M. *et al.* No association between variation in longevity candidate genes and aging-related phenotypes in oldest-old Danes. *Exp Gerontol* **78**, 57–61 (2016).
13. Hook, M. *et al.* Genetic cartography of longevity in humans and mice: Current landscape and horizons. *Biochim Biophys Acta Mol Basis Dis* **1864**, 2718–2732 (2018).
14. Huang, W. *et al.* Context-dependent genetic architecture of *Drosophila* life span. *PLoS Biol* **18**, e3000645 (2020).
15. Di Francesco, A. *et al.* Dietary restriction impacts health and lifespan of genetically diverse mice. *Nature* **634**, 684–692 (2024).
16. de Magalhães, J. P. Distinguishing between driver and passenger mechanisms of aging. *Nat Genet* **56**, 204–211 (2024).
17. De Benedictis, G. *et al.* Recent advances in human gene–longevity association studies. *Mechanisms of Ageing and Development* **122**, 909–920 (2001).
18. Deelen, J. *et al.* A meta-analysis of genome-wide association studies identifies multiple longevity genes. *Nat Commun* **10**, 3669 (2019).
19. Willcox, B. J., Willcox, D. C. & Ferrucci, L. Secrets of healthy aging and longevity from exceptional survivors around the globe: Lessons from octogenarians to supercentenarians. *J Gerontol A Biol Sci Med Sci* **63**, 1181–1185 (2008).
20. Gierman, H. J. *et al.* Whole-genome sequencing of the world's oldest people. *PLoS One* **9**, e112430 (2014).
21. Fortney, K. *et al.* Genome-wide scan informed by age-related disease identifies loci for exceptional human longevity. *PLoS Genet* **11**, e1005728 (2015).
22. McDaid, A. F. *et al.* Bayesian association scan reveals loci associated with human lifespan and linked biomarkers. *Nat Commun* **8**, 15842 (2017).
23. Timmers, P. R. *et al.* Genomics of 1 million parent lifespans implicates novel pathways and common diseases and distinguishes survival chances. *Elife* **8**, e39856 (2019).
24. Arias, E., Xu, J. & Kochanek, K. United States life tables, 2021.
25. Cottam, N. C. *et al.* From circuits to lifespan: translating mouse and human timelines with neuroimaging based tractography. *bioRxiv* 2024.07.28.605528 (2024) doi:10.1101/2024.07.28.605528.
26. Pletcher, S. D., Houle, D. & Curtsinger, J. W. Age-specific properties of spontaneous mutations affecting mortality in Drosophila melanogaster. *Genetics* **148**, 287–303 (1998).
27. Leips, J. & Mackay, T. F. C. The complex genetic architecture of *Drosophila* life span. *Exp Aging Res* **28**, 361–390 (2002).
28. Khazaeli, A. A. & Curtsinger, J. W. Pleiotropy and life history evolution in *Drosophila melanogaster*: uncoupling life span and early fecundity. *J Gerontol A Biol Sci Med Sci* **68**, 546–553 (2013).

29. Spencer, C. C. & Promislow, D. E. L. Age-specific changes in epistatic effects on mortality eate in *Drosophila melanogaster*. *Journal of Heredity* **96**, 513–521 (2005).
30. Herskind, A. M. *et al.* The heritability of human longevity: A population-based study of 2872 Danish twin pairs born 1870–1900. *Hum Genet* **97**, 319–323 (1996).
31. Hjelmborg, J. vB. *et al.* Genetic influence on human lifespan and longevity. *Hum Genet* **119**, 312–321 (2006).
32. Miller, R. A. *et al.* An Aging Interventions Testing Program: Study design and interim report. *Aging Cell* **6**, 565–575 (2007).
33. Harrison, D. E. *et al.* Rapamycin fed late in life extends lifespan in genetically heterogeneous mice. *Nature* **460**, 392–395 (2009).
34. Strong, R. *et al.* Lifespan benefits for the combination of rapamycin plus acarbose and for captopril in genetically heterogeneous mice. *Aging Cell* **21**, e13724 (2022).
35. Roderick, T. H. & Storer, J. B. Correlation between mean litter size and mean life span among 12 inbred strains of mice. *Science* **134**, 48–49 (1961).
36. Yuan, R., Flurkey, K., Meng, Q., Astle, M. C. & Harrison, D. E. Genetic regulation of life span, metabolism, and body weight in Pohn, a new wild-derived mouse strain. *J Gerontol A Biol Sci Med Sci* **68**, 27–35 (2013).
37. Auton, A. *et al.* A global reference for human genetic variation. *Nature* **526**, 68–74 (2015).
38. Bou Sleiman, M. *et al.* Sex- and age-dependent genetics of longevity in a heterogeneous mouse population. *Science* **377**, eabo3191 (2022).
39. Miller, R. A. Biomarkers of aging. *Science of Aging Knowledge Environment* (2001), 10.1126/sageke.2001.1.pe2
40. Medawar, P. B. (Peter B. *The Uniqueness of the Individual*. (New York, Basic Books, 1957).
41. Williams, G. C. & Taylor, P. D. Demographic consequences of natural selection. in *Evolution of Longevity in Animals: A Comparative Approach* (eds. Woodhead, A. D. & Thompson, K. H.) 235–245 (Springer US, Boston, MA, 1987). doi:10.1007/978-1-4613-1939-9_17.
42. Charlesworth, B. *Evolution in Age-Structured Populations*. (Cambridge University Press, Cambridge, 1980).
43. Kirkwood, T. B. L. Evolution of ageing. *Nature* **270**, 301–304 (1977).
44. Kirkwood, T. B. L., Rose, M. R., Harvey, P. H., Partridge, L. & Southwood, S. R. Evolution of senescence: late survival sacrificed for reproduction. *Philosophical Transactions of the Royal Society of London. Series B: Biological Sciences* **332**, 15–24 (1997).
45. Manichaikul, A., Dupuis, J., Sen, Ś. & Broman, K. W. Poor performance of bootstrap confidence intervals for the location of a quantitative trait locus. *Genetics* **174**, 481–489 (2006).
46. Nelson, J. F., Latham, K. R. & Finch, C. E. Plasma testosterone levels in C57BL/6J male mice: Effects of age and disease. *Acta Endocrinol (Copenh)* **80**, 744–752 (1975).
47. Bronson, F. H. & Desjardins, C. Reproductive failure in aged CBF1 male mice: Interrelationships between pituitary gonadotropic hormones, testicular function, and mating success. *Endocrinology* **101**, 939–945 (1977).
48. Schmidt, J. A., Oatley, J. M. & Brinster, R. L. Female mice delay reproductive aging in males. *Biol Reprod* **80**, 1009–1014 (2009).
49. Baud, A. *et al.* Genetic variation in the social environment contributes to health and disease. *PLoS Genet* **13**, e1006498 (2017).
50. Clutton-Brock, T. H. & Isvaran, K. Sex differences in ageing in natural populations of vertebrates. *Proc Biol Sci* **274**, 3097–3104 (2007).
51. Sapolsky, R. M. The influence of social hierarchy on primate health. *Science* **308**, 648–652 (2005).
52. Gesquiere, L. R. *et al.* Life at the top: rank and stress in wild male baboons. *Science* **333**, 357–360 (2011).
53. Razzoli, M. *et al.* Social stress shortens lifespan in mice. *Aging Cell* **17**, e12778 (2018).
54. Austad, S. N. & Fischer, K. E. Sex differences in lifespan. *Cell Metab* **23**, 1022–1033 (2016).
55. Manser, A., Lindholm, A. K., König, B. & Bagheri, H. C. Polyandry and the decrease of a selfish genetic element in a wild house mouse population. *Evolution* **65**, 2435–2447 (2011).
56. Kannisto, V., Turpeinen, O. & Nieminen, M. Finnish life tables since 1751. *Demogr Res* **1**, [28] p. (1999).
57. Mackay, T. F. C. Epistasis and quantitative traits: Using model organisms to study gene-gene interactions. *Nat Rev Genet* **15**, 22–33 (2014).

58. Chippindale, A. K., Gibson, J. R. & Rice, W. R. Negative genetic correlation for adult fitness between sexes reveals ontogenetic conflict in *Drosophila*. *Proc Natl Acad Sci U S A* **98**, 1671–1675 (2001).
59. Zhu, C. *et al.* Amplification is the primary mode of gene-by-sex interaction in complex human traits. *Cell Genom* **3**, 100297 (2023).
60. Cole, J. M. *et al.* The battle of the sexes in humans is highly polygenic. *Proc Natl Acad Sci U S A* **121**, e2412315121 (2024).
61. Vieira, C. *et al.* Genotype-environment interaction for quantitative trait loci affecting life span in *Drosophila melanogaster*. *Genetics* **154**, 213–227 (2000).
62. Rice, W. R. & Chippindale, A. K. Sexual recombination and the power of natural selection. *Science* **294**, 555–559 (2001).
63. Muir, C. D. & Moyle, L. C. Antagonistic epistasis for ecophysiological trait differences between Solanum species. *New Phytol* **183**, 789–802 (2009).
64. Kondrashov, A. S. Deleterious mutations and the evolution of sexual reproduction. *Nature* **336**, 435–440 (1988).
65. Desai, M. M., Weissman, D. & Feldman, M. W. Evolution can favor antagonistic epistasis. *Genetics* **177**, 1001–1010 (2007).
66. Ingram, D. K., Reynolds, M. A. & Les, E. P. The relationship of genotype, sex, body weight, and growth parameters to lifespan in inbred and hybrid mice. *Mech Ageing Dev* **20**, 253–266 (1982).
67. Miller, R. A., Harper, J. M., Galecki, A. & Burke, D. T. Big mice die young: early life body weight predicts longevity in genetically heterogeneous mice. *Aging Cell* **1**, 22–29 (2002).
68. Cheng, C. J., Gelfond, J. A. L., Strong, R. & Nelson, J. F. Genetically heterogeneous mice exhibit a female survival advantage that is age- and site-specific: Results from a large multi-site study. *Aging Cell* **18**, e12905 (2019).
69. Liu, J. *et al.* The complete telomere-to-telomere sequence of a mouse genome. *Science* **386**, 1141–1146 (2024).
70. Houtkooper, R. H. *et al.* Mitonuclear protein imbalance as a conserved longevity mechanism. *Nature* **497**, 451–457 (2013).
71. Joshi, P. K. *et al.* Genome-wide meta-analysis associates HLA-DQA1/DRB1 and LPA and lifestyle factors with human longevity. *Nat Commun* **8**, 910 (2017).
72. de Magalhães, J. P. *et al.* Human ageing genomic resources: Updates on key databases in ageing research. *Nucleic Acids Res* **52**, D900–D908 (2024).
73. Palmer, D. *et al.* Ageing transcriptome meta-analysis reveals similarities and differences between key mammalian tissues. *Aging (Albany NY)* **13**, 3313–3341 (2021).
74. Smith, G. S. & Walford, R. L. Influence of the main histocompatibility complex on ageing in mice. *Nature* **270**, 727–729 (1977).
75. Dear, K. B. *et al.* Traits that influence longevity in mice: a second look. *Genetics* **132**, 229–239 (1992).
76. Davis, E. J., Lobach, I. & Dubal, D. B. Female XX sex chromosomes increase survival and extend lifespan in aging mice. *Aging Cell* **18**, e12871 (2019).
77. Stevens, T. H. & Forgac, M. Structure, function and regulation of the vacuolar (H+)-ATPase. *Annu Rev Cell Dev Biol* **13**, 779–808 (1997).
78. Landis, G. N., Bhole, D. & Tower, J. A search for doxycycline-dependent mutations that increase Drosophila melanogaster life span identifies the VhaSFD, Sugar baby, filamin, fwd and Cctl genes. *Genome Biol* **4**, R8 (2003).
79. Yang, S. *et al.* ATP6V1H deficiency impairs glucose tolerance by augmenting endoplasmic reticulum stress in high fat diet fed mice. *Arch Biochem Biophys* **716**, 109116 (2022).
80. Ferraj, A. *et al.* Resolution of structural variation in diverse mouse genomes reveals chromatin remodeling due to transposable elements. *Cell Genom* **3**, 100291 (2023).
81. Palliyaguru, D. L. *et al.* Study of Longitudinal Aging in Mice: Presentation of Experimental Techniques. *J Gerontol A Biol Sci Med Sci* **76**, 552–560 (2021).
82. Jackson, A. U., Galecki, A. T., Burke, D. T. & Miller, R. A. Mouse loci associated with life span exhibit sex-specific and epistatic effects. *J Gerontol A Biol Sci Med Sci* **57**, B9–B15 (2002).
83. Roy, S. *et al.* Gene-by-environment modulation of lifespan and weight gain in the murine BXD family. *Nat Metab* **3**, 1217–1227 (2021).
84. Roy, S. *et al.* Charting the genetic loci linked to lifespan and variable response to the high fat diet in the BXD family. in *Abstracts CTC-RG2023* (2023).

85. Kolishovski, G. *et al.* The JAX Synteny Browser for mouse-human comparative genomics. *Mamm Genome* **30**, 353–361 (2019).
86. Hsu, A.-L., Feng, Z., Hsieh, M.-Y. & Xu, X. Z. S. Identification by machine vision of the rate of motor activity decline as a lifespan predictor in *C. elegans*. *Neurobiol Aging* **30**, 1498–1503 (2009).
87. Newell Stamper, B. L. *et al.* Movement decline across lifespan of *Caenorhabditis elegans* mutants in the insulin/insulin-like signaling pathway. *Aging Cell* **17**, e12704 (2018).
88. Kenyon, C., Chang, J., Gensch, E., Rudner, A. & Tabtiang, R. A *C. elegans* mutant that lives twice as long as wild type. *Nature* **366**, 461–464 (1993).
89. Zhu, J. & Chen, X. MCG10, a novel p53 target gene that encodes a KH domain RNA-binding protein, is capable of inducing apoptosis and cell cycle arrest in G(2)-M. *Mol Cell Biol* **20**, 5602–5618 (2000).
90. Ito, Y. *et al.* Suppression of poly(rC)-binding protein 4 (PCBP4) reduced cisplatin resistance in human maxillary cancer cells. *Sci Rep* **5**, 12360 (2015).
91. Yan, W. *et al.* Mice deficient in poly(C)-binding protein 4 are susceptible to spontaneous tumors through increased expression of ZFP871 that targets p53 for degradation. *Genes Dev* **30**, 522–534 (2016).
92. Chuang, T.-D. *et al.* Human prostatic acid phosphatase, an authentic tyrosine phosphatase, dephosphorylates ErbB-2 and regulates prostate cancer cell growth. *J Biol Chem* **285**, 23598–23606 (2010).
93. Quintero, I. B. *et al.* Transmembrane prostatic acid phosphatase (TMPAP) interacts with snapin and deficient mice develop prostate adenocarcinoma. *PLoS One* **8**, e73072 (2013).
94. Zeng, Z. *et al.* Acylpeptide hydrolase is a component of the cellular response to DNA damage. *DNA Repair (Amst)* **58**, 52–61 (2017).
95. Pandey, A. K., Lu, L., Wang, X., Homayouni, R. & Williams, R. W. Functionally enigmatic genes: a case study of the brain ignorome. *PLoS One* **9**, e88889 (2014).
96. Pasyukova, E. G., Vieira, C. & Mackay, T. F. Deficiency mapping of quantitative trait loci affecting longevity in Drosophila melanogaster. *Genetics* **156**, 1129–1146 (2000).
97. Leips, J. & Mackay, T. F. C. The complex genetic architecture of *Drosophila* life span. *Exp Aging Res* **28**, 361–390 (2002).
98. Bou Sleiman, M. *et al.* Sex- and age-dependent genetics of longevity in a heterogeneous mouse population. *Science* **377**, eabo3191 (2022).
99. Finch, C. *Longevity, Senescence and the Genome*. (The University of Chicago press, Chicago London, 1994).
100. Partridge, L. & Harvey, P. H. The ecological context of life history evolution. *Science* **241**, 1449–1455 (1988).
101. Kirkwood, T. B. & Austad, S. N. Why do we age? *Nature* **408**, 233–238 (2000).
102. Manton, K. G. & Vaupel, J. W. Survival after the age of 80 in the United States, Sweden, France, England, and Japan. *N Engl J Med* **333**, 1232–1235 (1995).
103. Newman, A. B. & Murabito, J. M. The epidemiology of longevity and exceptional survival. *Epidemiol Rev* **35**, 181–197 (2013).
104. Jiang, N. & Nelson, J. F. Sex Differences in mouse longevity and responses to geroprotective drugs: Implications for human intervention. *Public Policy Aging Rep* **33**, 120–124 (2023).
105. Arends, D. *et al.* Correlation trait loci (CTL) mapping: phenotype network inference subject to genotype. *Journal of Open Source Software* **1**, 87 (2016).
106. Williams, G. C. Pleiotropy, natural selection, and the evolution of senescence. *Evolution* **11**, 398–411 (1957).
107. Haldane, J., B. S. *New Paths in Genetics*. (George Allen & Uwin, London, 1941).
108. Maturana, H. R. & Valera, F. J. *Autopoiesis and Cognition. The Realization of the Living*. vol. 42 (D. Reidel Publishing Company, 1980).
109. MacArthur, R. H. & Wilson, E. O. *The Theory of Island Biogeography. (Princeton University Press*, 2001).
110. Eisenberg, J. F. *The Mammalian Radiations: An Analysis of Trends in Evolution, Adaptation, and Behavior*. (Chicago : University of Chicago Press, 1981).
111. Rose, M. R. Antagonistic pleiotropy, dominance, and genetic variation. *Heredity* **48**, 63–78 (1982).
112. Kirkwood, T. B. The disposable soma theory of aging. in *Genetic Effects on Aging II* 9–19 (Telford Press, Caldwell, N.J, 1990).
113. Rose, M. R. & Charlesworth, B. Genetics of life history in *Drosophila melanogaster*. I. Sib analysis of adult females. *Genetics* **97**, 173–186 (1981).

114. Rose, M. R. & Charlesworth, B. Genetics of life history in *Drosophila melanogaster*. II. Exploratory selection experiments. *Genetics* **97**, 187–196 (1981).
115. Leips, J. & Mackay, T. F. Quantitative trait loci for life span in *Drosophila melanogaster*: interactions with genetic background and larval density. *Genetics* **155**, 1773–1788 (2000).
116. König, B. & Lindholm, A. K. The complex social environment of female house mice (*Mus domesticus*). in *Evolution of the House Mouse* (eds. Piálek, J., Macholán, M., Munclinger, P. & Baird, S. J. E.) 114–134 (Cambridge University Press, Cambridge, 2012). doi:10.1017/CBO9781139044547.007.
117. Bronson, F. The reproductive ecology of the house mouse. *The Quarterly Review of Biology* **54**, 265–299 (1979).
118. Lipman, R., Galecki, A., Burke, D. T. & Miller, R. A. Genetic loci that influence cause of death in a heterogeneous mouse stock. *J Gerontol A Biol Sci Med Sci* **59**, 977–983 (2004).
119. Mitchell, S. J. *et al.* Effects of sex, strain, and energy intake on hallmarks of aging in mice. *Cell Metab* **23**, 1093–1112 (2016).
120. Mozhui, K. *et al.* Dissection of a QTL hotspot on mouse distal chromosome 1 that modulates neurobehavioral phenotypes and gene expression. *PLoS Genet* **4**, e1000260 (2008).
121. Wang, X. *et al.* Joint mouse-human phenome-wide association to test gene function and disease risk. *Nat Commun* **7**, 10464 (2016).
122. Allayee, H. *et al.* Systems genetics approaches for understanding complex traits with relevance for human disease. *Elife* **12**, e91004 (2023).
123. Herskind, A. M. *et al.* The heritability of human longevity: A population-based study of 2872 Danish twin pairs born 1870-1900. *Hum Genet* **97**, 319–323 (1996).
124. Garagnani, P. *et al.* Whole-genome sequencing analysis of semi-supercentenarians. *Elife* **10**, e57849 (2021).
125. Baud, A., McPeek, S., Chen, N. & Hughes, K. A. Indirect genetic effects: A cross-disciplinary perspective on empirical studies. *J Hered* **113**, 1–15 (2022).
126. Miller, R. A. *et al.* Rapamycin, but not resveratrol or simvastatin, extends life span of genetically heterogeneous mice. *J Gerontol A Biol Sci Med Sci* **66**, 191–201 (2011).
127. Miller, R. A. *et al.* Rapamycin-mediated lifespan increase in mice is dose and sex dependent and metabolically distinct from dietary restriction. *Aging Cell* **13**, 468–477 (2014).
128. Strong, R. *et al.* Nordihydroguaiaretic acid and aspirin increase lifespan of genetically heterogeneous male mice. *Aging Cell* **7**, 641–650 (2008).
129. Strong, R. *et al.* Longer lifespan in male mice treated with a weakly estrogenic agonist, an antioxidant, an α-glucosidase inhibitor or a Nrf2-inducer. *Aging Cell* **15**, 872–884 (2016).
130. Strong, R. *et al.* Rapamycin-mediated mouse lifespan extension: Late-life dosage regimes with sex-specific effects. *Aging Cell* **19**, e13269 (2020).
131. Harrison, D. E. *et al.* 17-a-estradiol late in life extends lifespan in aging UM-HET3 male mice; nicotinamide riboside and three other drugs do not affect lifespan in either sex. *Aging Cell* **20**, e13328 (2021).
132. Harrison, D. E. *et al.* Acarbose improves health and lifespan in aging HET3 mice. *Aging Cell* **18**, e12898 (2019).
133. Harrison, D. E. *et al.* Astaxanthin and meclizine extend lifespan in UM-HET3 male mice; fisetin, SG1002 (hydrogen sulfide donor), dimethyl fumarate, mycophenolic acid, and 4-phenylbutyrate do not significantly affect lifespan in either sex at the doses and schedules used. *GeroScience* (2023) doi:10.1007/s11357-023-01011-0.
134. Jiang, N. *et al.* Deciphering the timing and impact of life-extending interventions: Temporal efficacy profiler distinguishes early, midlife, and senescence phase efficacies. 2024.03.27.585737 Preprint at https://doi.org/10.1101/2024.03.27.585737 (2024).
135. Bitto, A. *et al.* Transient rapamycin treatment can increase lifespan and healthspan in middle-aged mice. *eLife* **5**, e16351 (2016).
136. Blagosklonny, M. V. Rapamycin for longevity: opinion article. *Aging (Albany NY)* **11**, 8048–8067 (2019).
137. Nadon, N. L., Strong, R., Miller, R. A. & Harrison, D. E. NIA Interventions Testing Program: Investigating putative aging intervention agents in a genetically heterogeneous mouse model. *EBioMedicine* **21**, 3–4 (2017).
138. Dutta, S. & Sengupta, P. Men and mice: Relating their ages. *Life Sci* **152**, 244–248 (2016).
139. Flurkey, K., Currer, J. M. & Harrison, D. E. *The Mouse in Biomedical Research - 2nd Edition*. vol. 3 (2007).

140. Gonzalez-Freire, M. *et al.* The road ahead for health and lifespan interventions. *Ageing Res Rev* **59**, 101037 (2020).
141. You, F. M. *et al.* BatchPrimer3: A high throughput web application for PCR and sequencing primer design. *BMC Bioinformatics* **9**, 253 (2008).
142. Nguyen-Dumont, T. *et al.* Hi-Plex for high-throughput mutation screening: application to the breast cancer susceptibility gene PALB2. *BMC Med Genomics* **6**, 48 (2013).
143. Langmead, B. & Salzberg, S. L. Fast gapped-read alignment with Bowtie 2. *Nat Methods* **9**, 357–359 (2012).
144. Li, H. *et al.* The Sequence Alignment/Map format and SAMtools. *Bioinformatics* **25**, 2078–2079 (2009).
145. Keane, T. M. *et al.* Mouse genomic variation and its effect on phenotypes and gene regulation. *Nature* **477**, 289–294 (2011).
146. Beierle, J. A. *et al.* Genetic basis of thermal nociceptive sensitivity and brain weight in a BALB/c reduced complexity cross. *Mol Pain* **18**, 17448069221079540 (2022).
147. Gabriel, S., Ziaugra, L. & Tabbaa, D. SNP genotyping using the Sequenom MassARRAY iPLEX platform. *Curr Protoc Hum Genet* **Chapter 2**, Unit 2.12 (2009).
148. Williams, R. W. The Portable Dictionary of the Mouse Genome: A personal database for gene mapping and molecular biology. *Mamm Genome* **5**, 372–375 (1994).
149. Sloan, Z. *et al.* GeneNetwork: framework for web-based genetics. *Journal of Open Source Software* **1**, 25 (2016).
150. Mulligan, M. K., Mozhui, K., Prins, P. & Williams, R. W. GeneNetwork: A Toolbox for systems genetics. *Methods Mol Biol* **1488**, 75–120 (2017).
151. Akeson, E. C. *et al.* Chromosomal inversion discovered in C3H/HeJ mice. *Genomics* **87**, 311–313 (2006).
152. Koenker, R., Chernozhukov, V., He, X. & Peng, L. *Handbook on Quantile Regression*. (Chapman and Hall/CRC, New York, 2017).
153. Therneau, T. M. *Modeling Survival Data: Extending the Cox Model*. (Springer, New York, 2000).
154. Broman, K. W. & Sen, S. *A Guide to QTL Mapping with R/Qtl*. (Springer, Dordrecht, 2009).
155. Arends, D., Prins, P., Jansen, R. C. & Broman, K. W. R/qtl: high-throughput multiple QTL mapping. *Bioinformatics* **26**, 2990–2992 (2010).
156. Broman, K. W., Wu, H., Sen, Ś. & Churchill, G. A. R/qtl: QTL mapping in experimental crosses. *Bioinformatics* **19**, 889–890 (2003).
157. Gao, X., Starmer, J. & Martin, E. R. A multiple testing correction method for genetic association studies using correlated single nucleotide polymorphisms. *Genet Epidemiol* **32**, 361–369 (2008).
158. Liu, Y. & Xie, J. Cauchy combination test: A powerful test with analytic p-value calculation under arbitrary dependency structures. *J Am Stat Assoc* **115**, 393–402 (2020).
159. Benjamini, Y., Drai, D., Elmer, G., Kafkafi, N. & Golani, I. Controlling the false discovery rate in behavior genetics research. *Behav Brain Res* **125**, 279–284 (2001).
160. Benjamini, Y. & Hochberg, Y. Controlling the false discovery rate: A practical and powerful approach to multiple testing. *Journal of the Royal Statistical Society: Series B (Methodological)* **57**, 289–300 (1995).
161. Falconer, D. S. *Introduction To Quantitative Genetics 4th Edition*. (1996).
162. Lynch, M. *Genetics and Analysis of Quantitative Traits*. (Sunderland, Mass. : Sinauer, 1998).
163. Kasprzyk, A. BioMart: driving a paradigm change in biological data management. *Database (Oxford)* **2011**, bar049 (2011).
164. McLaren, W. *et al.* The Ensembl variant effect predictor. *Genome Biol* **17**, 122 (2016).
165. de Magalhães, J. P. *et al.* The human ageing genomic resources: Online databases and tools for biogerontologists. *Aging Cell* Preprint at https://doi.org/10.1111/j.1474-9726.2008.00442.x (2009).
166. Elizarraras, J. M. *et al.* WebGestalt 2024: faster gene set analysis and new support for metabolomics and multi-omics. *Nucleic Acids Res* **52**, W415–W421 (2024).
167. Kim, W., Underwood, R. S., Greenwald, I. & Shaye, D. D. OrthoList 2: A new comparative genomic analysis of human and *Caenorhabditis elegans* genes. *Genetics* **210**, 445–461 (2018).
168. Fraser, A. G. *et al.* Functional genomic analysis of *C. elegans* chromosome I by systematic RNA interference. *Nature* **408**, 325–330 (2000).

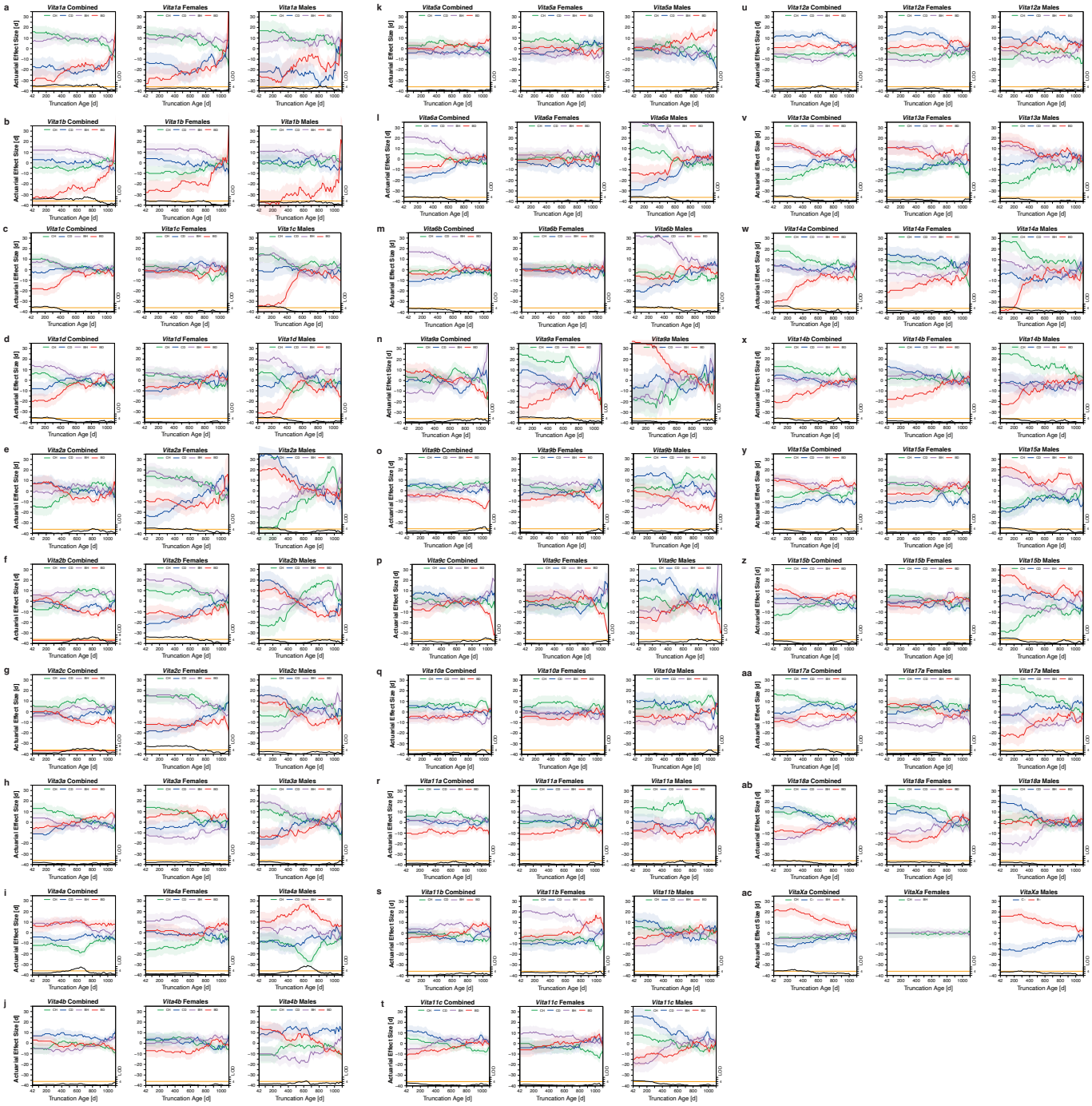

Extended Data Fig. 1 | *Vita* loci genotype effect plots. Trios of effect size plots as described in detail in the legend to Figs 1 and 2. Each trio plots combined data for both sexes (left), for females (middle), and for males (right). To understand genetic sources that may account from timing changes in mortality rates it is helpful to compare these more complex genotype plot to pairs of haplotype plots reproduced in Extended Data Fig. 2.

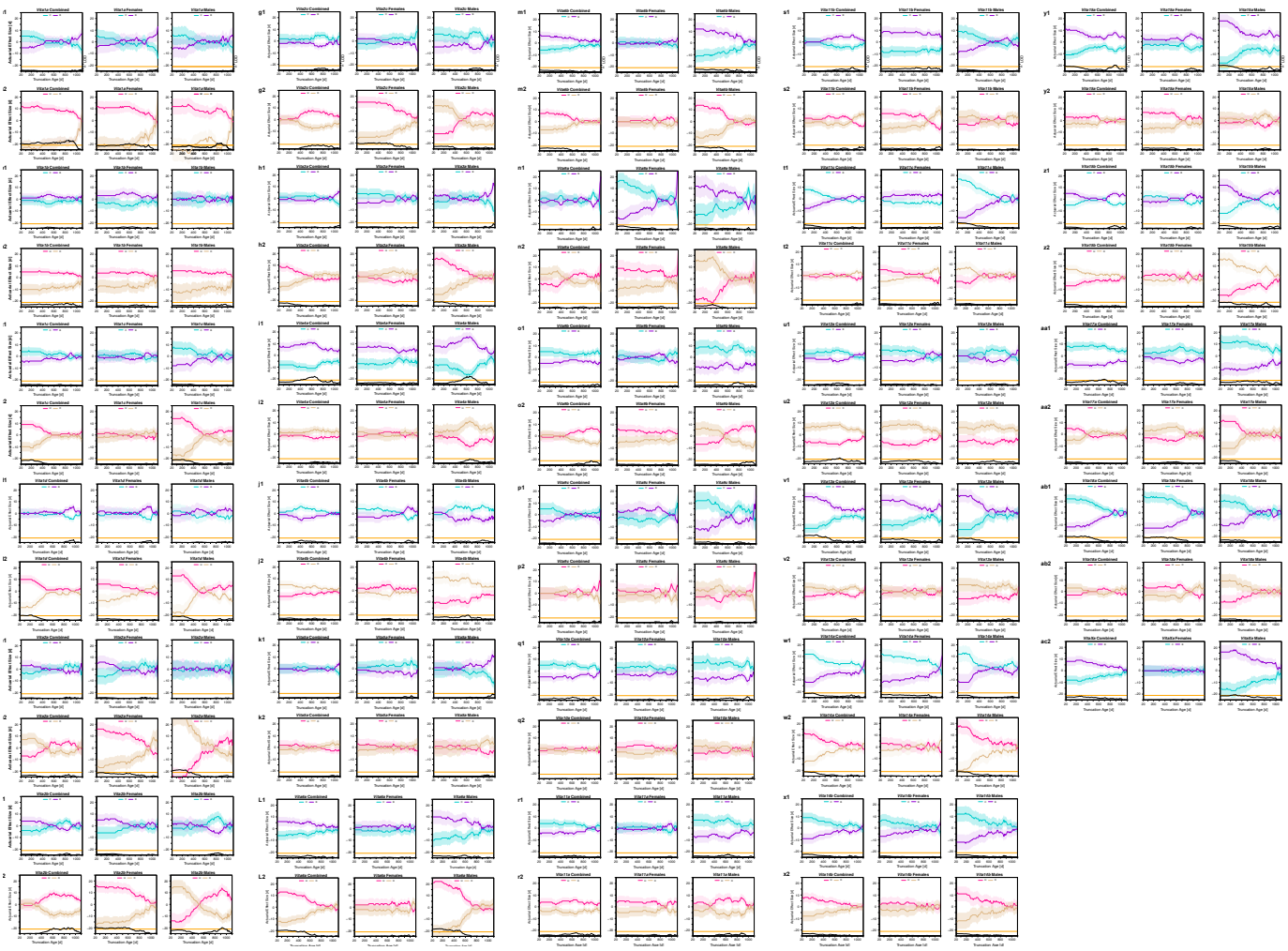

Extended Data Fig. 2 | *Vita* loci haplotype effect plots. Pair of trios of effect size plots for the haplotypes of each *Vita* locus. The upper trio (blue and purple shades) give differences in actuarial effects for the maternal haplotypes—*C* and *B*. The lower trio (pink and beige shads) give differences for the paternal haplotypes—*H* and *D*. Each of these plots is symmetric around the mean and easier to interpret than the matched genotype plots in Extended Data Fig. 1. However, these plots generally have lower LOD scores.

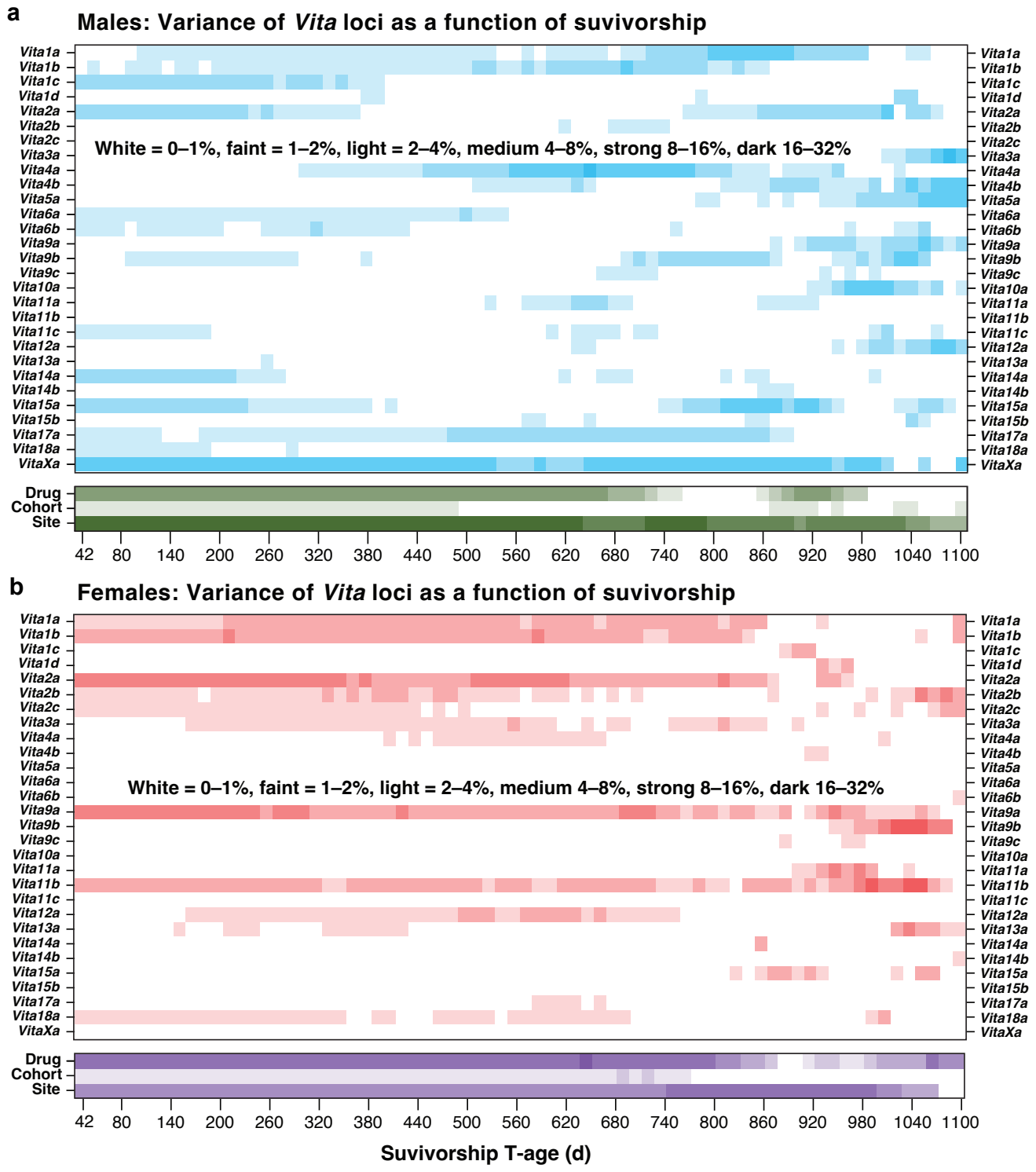

Extended data Fig. 3 | Dynamics and variance of 29 *Vita* loci as a function of sex and survivorship. Variance was estimated for each survivorship and sex: males in blue in **(a)** and females in red in **(b)** with intensity of colors indicating levels of the variance explained, where white = 0–1%, faint = 1–2%, light = 2–4%, medium 4–8%, strong 8–16%, dark 16–32%. The non-genetic sources of variance (**Ve**) are provided in green for males and purple for females. **Drug** is variance attributable to multiple nominally ineffective supplementary drug treatments versus the standard chow diet. **Cohort** is variance attributable to the annual cycles of production of UM-HET3 mice from late spring through late fall between 2004 and 2013 (2008 was a hiatus year, and 2012 and 2013 only included mice from UM). **Site** is variance associated with the three ITP colony sites: The Jackson Laboratory, The University of Michigan, and University of Texas Health San Antonio. Compare this figure with Jiang et al. (Ref. 133) in which the impact of drug interventions are places on a similar time scale.

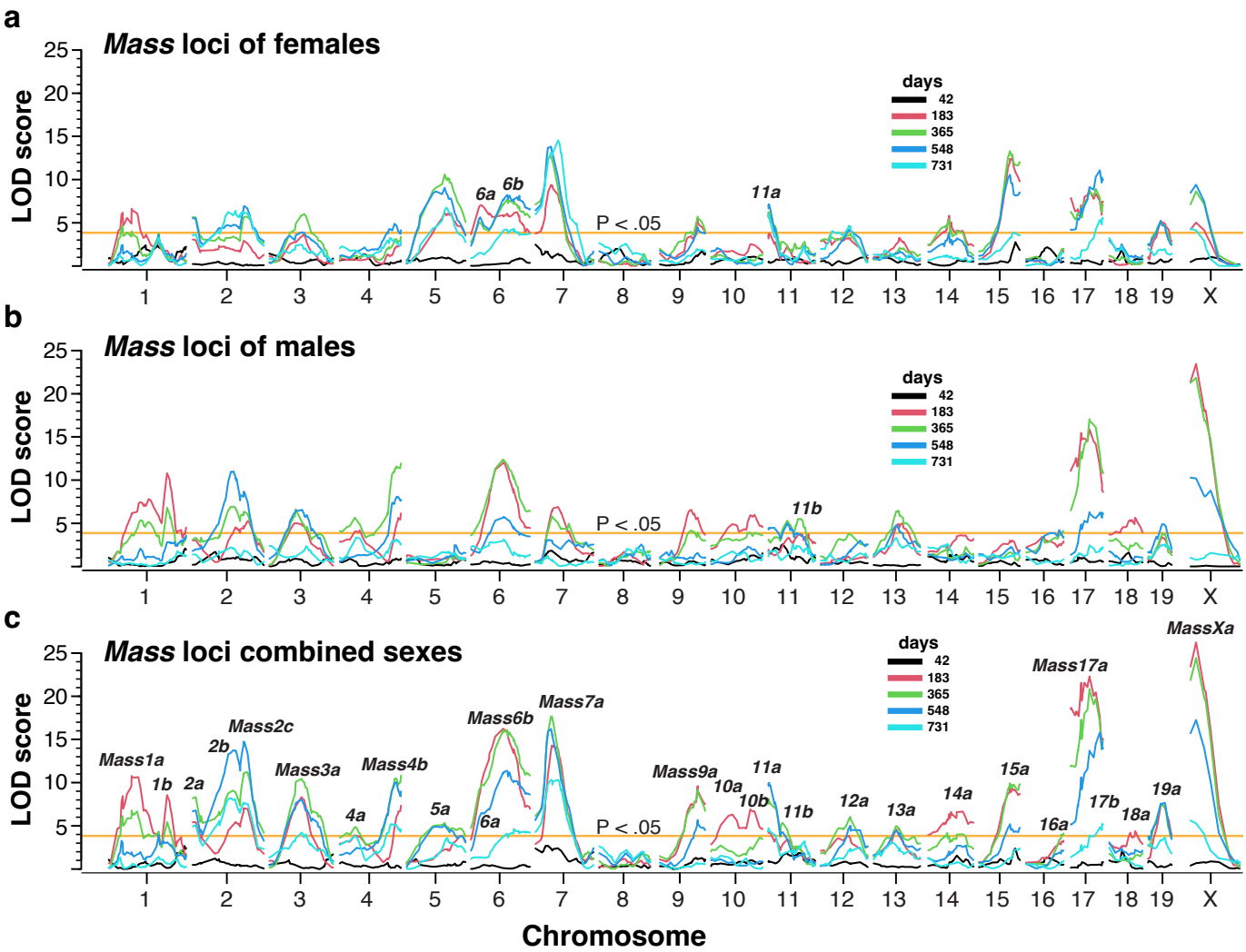

d

Age Weighed (days)	Sample Size by Sex and Site (n)					
	Male	Female	JL*	UM*	UT*	Sum
42	1369	1090	915	901	643	2459
183	2388	2167	1577	2072	1039	4688
365	2241	2050	1601	1701	998	4300
548	2127	2103	1394	1927	910	4231
730	1006	1201	793	951	464	2208

* JL = The Jackson Laboratory. UM = University of Michigan.
UT = University of Texas Health Science Center at San Antonio

Extended Data Fig. 4 | Body *Mass* loci at five ages. **a,** Female maps. **b,** Male maps. **c,** Combined maps in which all significant *Mass* loci have been labeled. Note that three of the 28 *Mass* loci are more distinct in the female map (*Mass6a*, *Mass6b*, and *Mass11a*) than in combined or male maps. *Mass11b* is more distinct in the male map. At all ages the mapping model compensates for drug treatment, cohort year, and site, and in the case of the combined sexes also adjusts for sex. Compare **(c)** with Fig. 5a, but note that color assignments are different here. **d,** Table of sample sizes for each sex and for the sites. The lower sample size at 730 days (~ 2 years) is primarily due to mortality before this age, that at 42 days because these early life weights were only obtained over the first four years of the program.

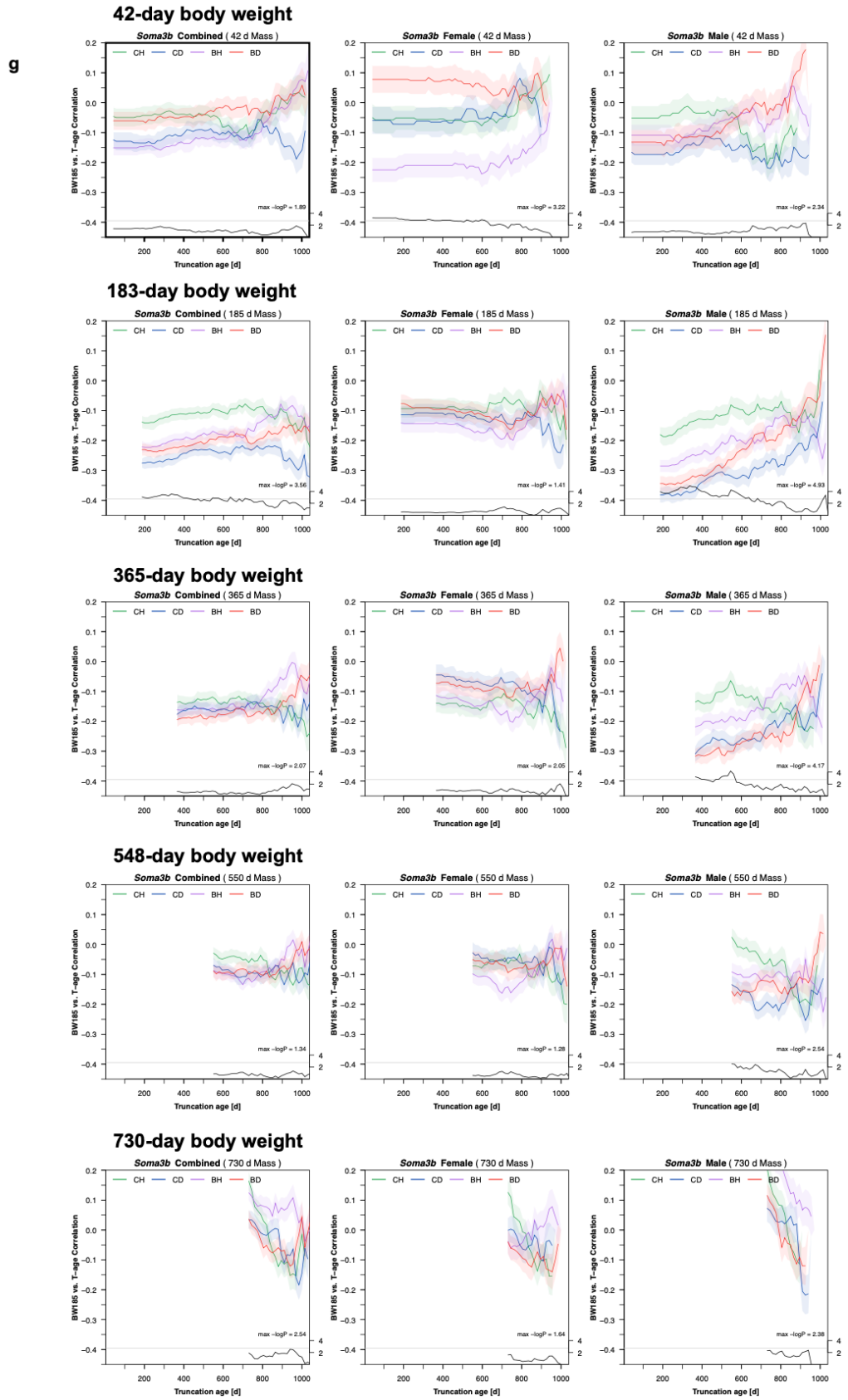

Extended Data Fig. 5a | *Soma* actuarial effect size plots. **a,** An example of one of 30 *Soma* loci full actuarial effect size plots. The original figure cannot be optimized as a single-page PDF and is best viewed within Inkscape or Adobe Illustrator so that readers can examine individual or sets of *Soma* loci. The figure consists of 30 layers of loci, aligned on top of each other. Each locus is given at the five ages at which mice were weighed. In this PDF version, we have reproduced only *Soma3b* (also see Fig. 5i,j for more context). In Extended Data Fig. 5b that follows, we illustrate the PDF of all 30 overlapping *Soma* loci.

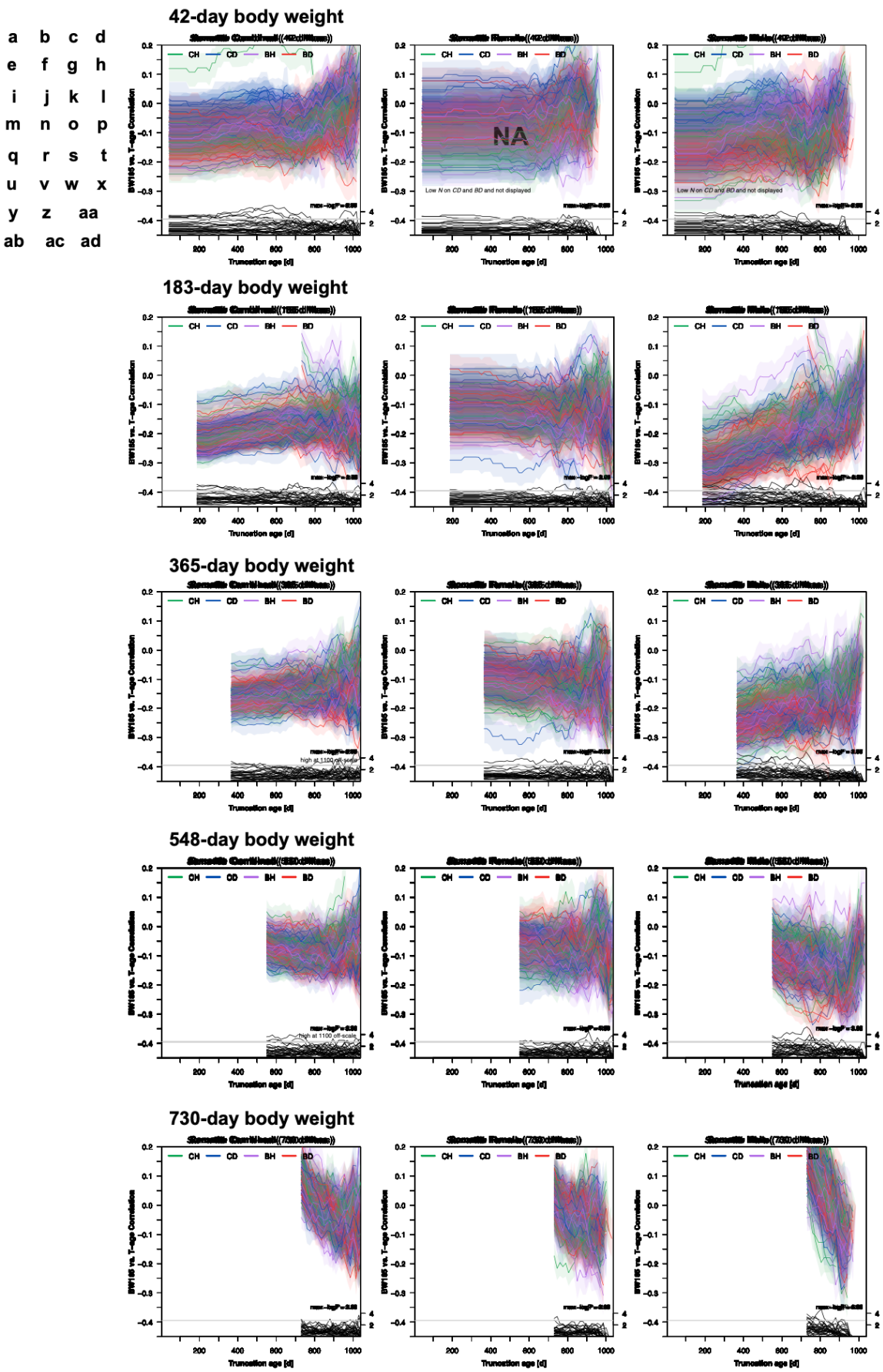

Extended Data Fig. 5b | *Soma* actuarial effect size plots. b, An overlay of plots of all 30 *Soma* loci. In Extended Data Fig. 5a, we reproduce just the *Soma3b* layer.